

## **6 Surface Wave Absorber Measurements**

### **6.1 Introduction**

Although soft boundaries form an electromagnetic superior solution for reducing the RCS resulting from edge diffracted waves, isotropic surface wave absorbers remain useful in many applications, even for RCS management of edge diffracted waves. For example, surface wave absorbers can be very effective in absorbing creeping waves when applied to the fuselage of a plane. Also, in the case of a surface discontinuity, there may be a problem with edge diffracted waves for one radar polarization only, depending on the nature of the surface discontinuity and its aspect angle. In such a case, an ordinary surface wave absorber (either E-type or H-type, depending on the case) would be a good substitute for a soft boundary. From this perspective it is obvious that there is a lot interest in determining the quality and efficacy of commercially available surface wave absorbers.

In order to fully characterize a surface wave absorber two physical quantities need to be measured: the attenuation constant  $\alpha$  and the phase constant  $\beta$ , both in the direction of propagation. However, the two quantities can be combined into one complex phase constant  $\beta = \beta' - j\beta'' = \beta' - j\alpha$ , as is done in this chapter. (See also Section 2.5.)

Many applications of surface wave absorbing materials are accompanied with propagation of surface waves over planar or near-planar surfaces. A test cell for surface wave absorbing materials should therefore be capable of reproducing the properties of infinite plane surface wave propagation without introducing any other propagation or scattering mechanisms.

## 6.2 A Historical Overview of Surface Wave Measurement Techniques

### 6.2.1 The Aperture Method

One of the few ways to generate a plane surface wave is depicted in Figure 6.1. The method was first suggested by Barlow and Cullen [1]<sup>1</sup> in as early as 1951 and is still in use today. The method is based on the theory presented in Section 3.4.7. There, it was shown that a coated PEC will support one or more surface wave modes for certain angles of incidence of an illuminating plane wave (Fig. 3.6). Parallel polarized incident waves will cause E-type surface waves to propagate along the coating, only when they are incident at angles which are solutions of (Snell's law substituted into (3.43))

$$R_{//} = \frac{\eta_2 \cos(\theta_{2i}) - j\eta_1 \sqrt{1 - \left[\frac{k_2}{k_1} \sin(\theta_{2i})\right]^2} \tan \left[ hk_1 \sqrt{1 - \left[\frac{k_2}{k_1} \sin(\theta_{2i})\right]^2} \right]}{\eta_2 \cos(\theta_{2i}) + j\eta_1 \sqrt{1 - \left[\frac{k_2}{k_1} \sin(\theta_{2i})\right]^2} \tan \left[ hk_1 \sqrt{1 - \left[\frac{k_2}{k_1} \sin(\theta_{2i})\right]^2} \right]} = 0.$$

H-type surface waves will result from perpendicular polarized waves incident at angles which are solutions of (Snell's law substituted into (3.44))

$$R_{\perp} = \frac{\frac{\cos(\theta_{2i})}{\eta_2} + j \frac{\sqrt{1 - \left[\frac{k_2}{k_1} \sin(\theta_{2i})\right]^2}}{\eta_1} \cot \left[ hk_1 \sqrt{1 - \left[\frac{k_2}{k_1} \sin(\theta_{2i})\right]^2} \right]}{\frac{\cos(\theta_{2i})}{\eta_2} - j \frac{\sqrt{1 - \left[\frac{k_2}{k_1} \sin(\theta_{2i})\right]^2}}{\eta_1} \cot \left[ hk_1 \sqrt{1 - \left[\frac{k_2}{k_1} \sin(\theta_{2i})\right]^2} \right]} = 0.$$

Also, note that the use of the term "Brewster angle" is inappropriate here.

<sup>1</sup> The paper contains some errors which have been corrected in this text.

An experimental set-up as shown in Figure 3.6 is insufficient if the field of the surface wave is to be measured by a probe. Not only the field of the surface wave will be present above the coating, but also the field of the incident wave. (See equation (3.37a).) Therefore, part of the coating needs to be shielded from the incident plane wave, as shown in Figure 6.1.

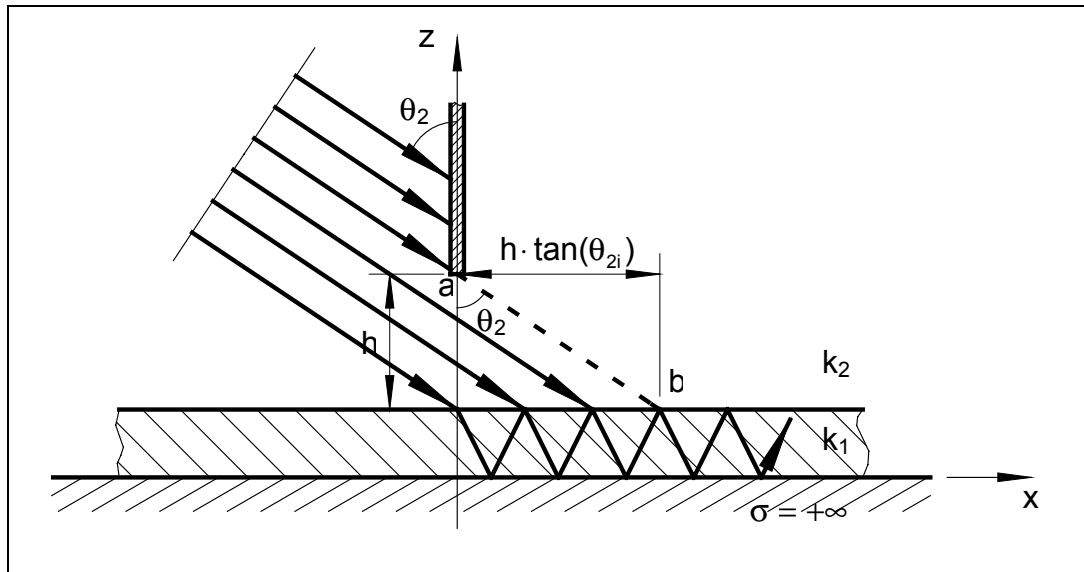


Figure 6.1: A method of generating plane surface waves (See text.)

If the wavelength is small compared with the height  $h$  of the aperture, ray-optics theory will give a first approximation to the effect of the screen, namely that below the shadow line  $ab$  there will be a plane wave travelling down into the coating, provided that the angle of incidence is chosen well. There will also be some surface wave energy in this region. The region right and above the shadow line  $ab$  will contain the field of the surface wave together with a small field contribution of diffracted waves coming from the edge of the aperture. Starting at a distance  $b = h \cdot \tan(\theta_{2i})$  away from the aperture, the field distribution near ground level will approximate that of a plane surface wave.

A probe is used to measure the field intensity at different positions of the aperture. From these measurements the surface wave attenuation over a certain length of coating can be calculated. To determine the wavelength of the surface wave, a reflecting wall is placed at the end of the coating and the distance between two consecutive (rectified) maxima of the standing wave pattern is measured. Twice this distance corresponds to the wavelength of the surface wave.

The measurement technique described in this section is not without any defects. Firstly, it is impossible to generate a plane wave; in practice, it can only be approximated. Secondly, it is extremely difficult to determine at what angle unknown coatings under test should be illuminated. Moreover, this angle is often complex, implying that the incident wave should be inhomogeneous. Also, the surface wave field can not be isolated because of diffraction mechanisms. Finally, a probe for measuring the surface wave field will always interfere with the field.

## 6.2.2 The Broad-Band Radial Surface Wave Antenna

A plane surface wave can also be approximated by a radial surface wave at a large distance from its point of excitation. Radial surface waves can easily be excited using a radial surface wave antenna as in Figure 6.2.

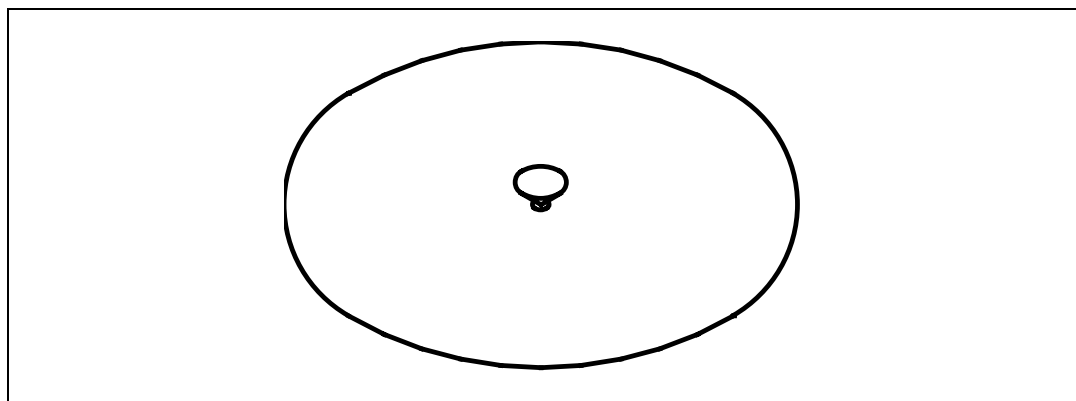


Figure 6.2: A broadband radial surface wave antenna; the groundplane diameter is about 1 meter

A similar set-up was used by Fernando and Barlow to make probe measurements of the surface wave field [2]. However, at The University of Hull this configuration has been used to obtain time domain data from reflection coefficient measurements in the frequency domain over the band 1GHz to 11GHz [3]. For this purpose, the cylindrical antenna described in [2] is replaced by a broad-band conical monopole antenna. The new antenna is optimized for broad-band performance and has a height of 50mm with a flare angle of  $90^\circ$ . (More information on designing conical monopoles can be found in [4].)

Frequency response or tracking error calibration is effected by measuring a coaxial line short circuit at the input to the conical monopole.

After calibration, two measurements can be performed. First, data is taken without coating the groundplane. The second measurement involves covering the groundplane with the material under test. For both measurements a peak in the time domain will occur at approximately  $t = \frac{2r}{v}$ , where  $r$  is the radius of the ground plane and  $v$  is the velocity of propagation. This peak in the time domain reflection coefficient data is caused by diffraction at the rim of the groundplane.

Only an average value of the phase constant  $\beta$  can be obtained by this technique because  $v$  is a function of frequency for the surface wave. Results are given in [3]. Also, the surface wave launching efficiency of the antenna and the reflection coefficient at the rim are unknown. Therefore, the attenuation data is only of qualitative value.

### 6.2.3 Loss Measurements of the Goubau-Line

Loss measurements of the Goubau-line are perhaps the most accurate surface wave loss measurements that have ever been made up to now. Clearly, the waves propagating along a Goubau-line are not plane surface waves but axial surface waves, which are easier to measure directly. Nonetheless, a lot can be learned from the techniques employed in these measurements.

Two methods have been reported that both refrain from using a probe to measure the surface wave field. In a first measurement technique [5], a Goubau-line resonator is formed by placing large circular plates at each end of the Goubau-line. The power is fed to and from the resonator by means of small coupling loops, one at each end plate. The attenuation of the Goubau-line is obtained by the determining the half power bandwidth of the surface wave resonator. The only thing that is somewhat cumbersome about this method is the fact that the resonator needs to be retuned for each measurement at a different frequency. Also, in order to obtain maximum accuracy, the insertion loss and mutual coupling of the coupling loops should be known.

In the other measurement method [6], an axial surface wave is launched on the Goubau-line at one end by means of a launching horn. At the other end, the Goubau-line is terminated by a movable short. Both the attenuation constant  $\alpha$  and the phase constant  $\beta$  can be inferred from two input impedance measurements with different line lengths. A third measurement with a line length shorter than in the previous measurements defines a phase reference plane to which the previous measurements are calibrated for frequency response (tracking error). Unlike the measurement techniques described earlier in this section, this method has no fundamental limitations. A technique very similar to this technique will be employed for measuring plane surface waves. This new technique will be presented in the next section.

## 6.3 A Plane Surface Wave Simulator Cell Based on a Partially Filled Rectangular Waveguide

### 6.3.1 Introduction

From the previous it has become clear that the generation of plane surface waves is not evident if also the presence of other propagating waves (e.g. the space wave and diffracted waves) has to be avoided. Moreover, in order to make accurate measurements, at least one surface wave calibration standard should be available.

It is, however, extremely difficult to meet the above-mentioned requirements with plane surface waves. Therefore, the new measurement technique here presented, will be based on the strategy of replacing the plane surface wave by another wave with similar properties but which suits itself better to attenuation and phase constant measurements. The waves propagating in a partially filled waveguide (Fig. 6.3) are proposed here as a replacement for the plane surface waves. A partially filled waveguide has the advantage of being completely shielded, and is hence less susceptible to noise and interference from the lab environment. When taken care for, only one mode will propagate inside the waveguide. Moreover, a short can be reproduced accurately and thus serve as a calibration standard.

Even from an intuitive approach can be seen that the waves propagating inside a partially filled waveguide of sufficient height have a lot in common with plane surface waves. In Chapter 3 was shown that, away from the material interface, the field of a surface wave decays exponentially. Putting a horizontal metallic wall (e.g. the upper wall of a waveguide) sufficiently high above the coated surface will influence the field of a plane surface wave only to a very small extent. Adding vertical metallic walls (e.g. those of a waveguide) will result in a sine or cosine dependence in the transversal direction for all field components. However, these additional sine or cosine factors are fully determined by the distance between the vertical walls (i.e. the width of the waveguide). The presence of vertical walls will also cause the complex phase constant  $\beta$  to be different from that of plane surface wave propagation. Again, this effect can easily be accounted for: the difference between both phase constants only depends upon the distance between the vertical walls. A rigorous proof for all statements made in this paragraph, will be given later in this chapter.

The complex phase constant of the wave in the partially filled waveguide can be inferred from input impedance measurements of the waveguide terminated by a short circuit at different positions.

The proposed measurement method will here only be validated for single layer materials that are linear, homogeneous and isotropic. There is however a high degree of similarity between the surface wave fields over single layer and multi-layer materials. For this reason it may be assumed that the measurement method presented in the section will be equally suited for the characterization of homogeneous linear isotropic multi-layer coatings.

### 6.3.2 The Partially Filled Rectangular Waveguide

The next two sections deal with the analysis of the waves propagating in a partially filled rectangular waveguide (Fig. 6.3) [7]. In this analysis, it will be assumed that the rectangular waveguide has perfectly conducting walls and that it is filled with two different media as depicted in Figure 6.3. The interface of these media is parallel with upper and lower wall of the rectangular waveguide. Both media are assumed to be homogeneous, linear and isotropic. The x-axis is chosen parallel with the propagation direction.

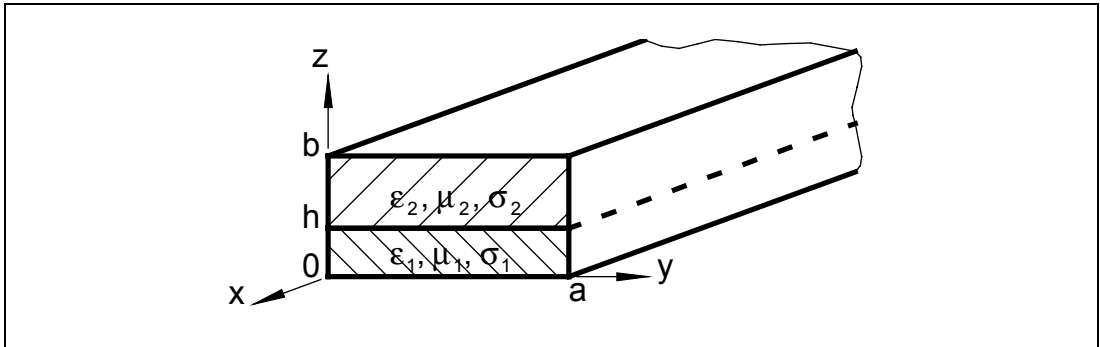


Figure 6.3: A partially filled rectangular waveguide; both media are assumed to be homogenous, linear and isotropic, the walls are perfectly conducting.

The partially filled rectangular waveguide is a 2D-uniform guiding structure. General Hertz potentials for 2D-uniform guiding structures were found in Section 2.5. Contrary to Chapter 3, the Hertz vector potential  $\vec{\Pi}$  will here not only depend on the z-coordinate, but the y-coordinate as well.

Therefore,

$$\vec{\Pi} = \Pi(y, z)e^{-j\beta_x x}\vec{e}_z. \quad (1)$$

while

$$u_1 = z; \quad u_2 = x; \quad u_3 = y.$$

Substituting (1) into (2.10) results in general expressions for the field components of E-type waves in one of the media

$$\begin{aligned}
 E_z &= k^2 \Pi_e + \frac{\partial^2 \Pi_e}{\partial z^2}; \quad H_z = 0, \\
 E_x &= -j\beta_x \frac{\partial \Pi_e}{\partial z}; \quad H_x = (\sigma + j\omega\epsilon) \frac{\partial \Pi_e}{\partial y}, \\
 E_y &= \frac{\partial^2 \Pi_e}{\partial z \partial y}; \quad H_y = j\beta_x (\sigma + j\omega\epsilon) \Pi_e.
 \end{aligned} \tag{2}$$

From (2) it can be seen that the E-type waves in a partially filled rectangular waveguide are longitudinal section magnetic (LSM) waves. The magnetic field intensity  $\vec{H}$  has no component in the direction normal to the material interface ( $H_z = 0$ ).

Substituting (1) into (2.11) leads general expressions for the field components of H-type waves in one of the media

$$\begin{aligned}
 H_z &= k^2 \Pi_m + \frac{\partial^2 \Pi_m}{\partial z^2}; \quad E_z = 0, \\
 H_x &= -j\beta_x \frac{\partial \Pi_m}{\partial z}; \quad E_x = -j\omega\mu \frac{\partial \Pi_m}{\partial y}, \\
 H_y &= \frac{\partial^2 \Pi_m}{\partial z \partial y}; \quad E_y = \beta_x \omega\mu \Pi_m.
 \end{aligned} \tag{3}$$

From (3) one can conclude that the H-type waves in a partially filled rectangular waveguide are longitudinal section electric (LSE) waves. The electric field intensity  $\vec{E}$  has no component in the direction normal to the material interface ( $E_z = 0$ ).

### 6.3.3 E-Type Waves in a Partially Filled Rectangular Waveguide

A suitable Hertz function for medium 1 that satisfies the boundary conditions

$$E_x = E_z = 0 \text{ at } y = 0 \text{ and } 0 < y < +\infty ,$$

$$E_x = E_y = 0 \text{ at } z = 0$$

$$\text{is } \Pi_1 = A_1 \sin(s_{y1}y) \cos(s_{z1}z) e^{-j\beta_x x} . \quad (4)$$

Introducing (4) into (2)

$$E_{z1} = A_1 (k_1^2 - s_{z1}^2) \sin(s_{y1}y) \cos(s_{z1}z) e^{-j\beta_x x} , \quad (5a)$$

$$E_{x1} = j\beta_x A_1 s_{z1} \sin(s_{y1}y) \sin(s_{z1}z) e^{-j\beta_x x} , \quad (5b)$$

$$E_{y1} = -A_1 s_{y1} s_{z1} \cos(s_{y1}y) \sin(s_{z1}z) e^{-j\beta_x x} , \quad (5c)$$

$$H_{z1} = 0 , \quad (5d)$$

$$H_{x1} = (\sigma_1 + j\omega\epsilon_1) A_1 s_{y1} \cos(s_{y1}y) \cos(s_{z1}z) e^{-j\beta_x x} , \quad (5e)$$

$$H_{y1} = j\beta_x (\sigma_1 + j\omega\epsilon_1) A_1 \sin(s_{y1}y) \cos(s_{z1}z) e^{-j\beta_x x} . \quad (5f)$$

An additional boundary condition is

$$E_x = E_z = 0 \text{ at } y = a .$$

$$\text{Hence, } s_{y1}a = n\pi \Rightarrow s_{y1} = \frac{n\pi}{a} \quad (6)$$

where n is a positive integer different from zero.

n=0 corresponds to the solution for a partially filled parallel plate waveguide.

A suitable Hertz function for medium 2 that satisfies the boundary conditions

$$E_x = E_z = 0 \text{ at } y = 0 \text{ and } 0 < y < +\infty ,$$

$$E_x = E_y = 0 \text{ at } z = b$$

$$\text{is } \Pi_2 = A_2 \sin(s_{y2}y) \cos[s_{z2}(z - b)] e^{-j\beta_x x} . \quad (7)$$

Introducing (7) into (2)

$$E_{z2} = A_2 (k_2^2 - s_{z2}^2) \sin(s_{y2}y) \cos[s_{z2}(z - b)] e^{-j\beta_x x} , \quad (8a)$$

$$E_{x2} = j\beta_x A_2 s_{z2} \sin(s_{y2}y) \sin[s_{z2}(z - b)] e^{-j\beta_x x} , \quad (8b)$$

$$E_{y2} = -A_2 s_{y2} s_{z2} \cos(s_{y2}y) \sin[s_{z2}(z - b)] e^{-j\beta_x x} , \quad (8c)$$

$$H_{z2} = 0 , \quad (8d)$$

$$H_{x2} = (\sigma_2 + j\omega\epsilon_2) A_2 s_{y2} \cos(s_{y2}y) \cos[s_{z2}(z - b)] e^{-j\beta_x x} , \quad (8e)$$

$$H_{y2} = j\beta_x (\sigma_2 + j\omega\epsilon_2) A_2 \sin(s_{y2}y) \cos[s_{z2}(z - b)] e^{-j\beta_x x} . \quad (8f)$$

An additional boundary condition is

$$E_x = E_z = 0 \text{ at } y = a .$$

$$\text{Hence, } s_{y2}a = n\pi \Rightarrow s_{y2} = \frac{n\pi}{a} . \quad (9)$$

By virtue of (2.13), (2.15), (6) and (9)

$$s_{y1}^2 + s_{z1}^2 = \left(\frac{n\pi}{a}\right)^2 + s_{z1}^2 = s_1^2 = k_1^2 - \beta_x^2 \Rightarrow s_{z1} = +\sqrt{k_1^2 - \left(\frac{n\pi}{a}\right)^2 - \beta_x^2}, \quad (10)$$

$$s_{y2}^2 + s_{z2}^2 = \left(\frac{n\pi}{a}\right)^2 + s_{z2}^2 = s_2^2 = k_2^2 - \beta_x^2 \Rightarrow s_{z2} = +\sqrt{k_2^2 - \left(\frac{n\pi}{a}\right)^2 - \beta_x^2}. \quad (11)$$

Choosing the negative square roots would have no effect on the results.

The tangential components of  $\vec{E}$  and  $\vec{H}$  are continuous across the interface of two media. Furthermore, it was shown that  $s_{y1} = s_{y2}$ .

Hence,

$$E_{x1} = E_{x2} \text{ and } E_{y1} = E_{y2} \text{ at } z = h$$

$$\Rightarrow A_1 s_{z1} \sin(s_{z1}h) = -A_2 s_{z2} \sin[s_{z2}(b-h)], \quad (12)$$

$$\text{as well as } H_{x1} = H_{x2} \text{ and } H_{y1} = H_{y2} \text{ at } z = h$$

$$\Rightarrow (\sigma_1 + j\omega\epsilon_1)A_1 \cos(s_{z1}h) = (\sigma_2 + j\omega\epsilon_2)A_2 \cos[s_{z2}(b-h)]. \quad (13)$$

Note that (12) and (13) would have resulted in a set of contradictory equations, if  $\vec{\Pi}$  were chosen in any direction other than the z-direction.

Dividing (12) by (13) yields

$$\frac{s_{z1}}{\sigma_1 + j\omega\epsilon_1} \tan(s_{z1}h) = -\frac{s_{z2}}{\sigma_2 + j\omega\epsilon_2} \tan[s_{z2}(b-h)] \quad (14)$$

or by virtue of (10) and (11)

$$\begin{aligned} & \frac{\sqrt{k_1^2 - \left(\frac{n\pi}{a}\right)^2 - \beta_x^2}}{\sigma_1 + j\omega\epsilon_1} \tan\left[h\sqrt{k_1^2 - \left(\frac{n\pi}{a}\right)^2 - \beta_x^2}\right] \\ &= -\frac{\sqrt{k_2^2 - \left(\frac{n\pi}{a}\right)^2 - \beta_x^2}}{\sigma_2 + j\omega\epsilon_2} \tan\left[(b-h)\sqrt{k_2^2 - \left(\frac{n\pi}{a}\right)^2 - \beta_x^2}\right] \end{aligned} \quad (15)$$

This dispersion equation is transcendental and can therefore only be solved numerically for  $\beta_x$ .

Letting  $h = 0$  in (15), results in

$\beta_x = \sqrt{k_2^2 - \left(\frac{n\pi}{a}\right)^2 - \left(\frac{m\pi}{b}\right)^2}$ , the dispersion equation of the  $TE_{nm}$  empty waveguide modes.

The dispersion equation for the  $TE_{nm}$  modes of the homogeneously filled waveguide is obtained by letting  $h=b$  in (15).

### 6.3.4 H-Type Waves in a Partially Filled Rectangular Waveguide

A suitable Hertz function for medium 1 that satisfies the boundary conditions

$$E_x = E_z = 0 \text{ at } y = 0 \text{ and } 0 < y < +\infty ,$$

$$E_x = E_y = 0 \text{ at } z = 0$$

$$\text{is } \Pi_1 = A_1 \cos(s_{y1}y) \sin(s_{z1}z) e^{-j\beta_x x} . \quad (17)$$

Introducing (17) into (3)

$$H_{z1} = A_1 (k_1^2 - s_{z1}^2) \cos(s_{y1}y) \sin(s_{z1}z) e^{-j\beta_x x} , \quad (18a)$$

$$H_{x1} = -j\beta_x A_1 s_{z1} \cos(s_{y1}y) \cos(s_{z1}z) e^{-j\beta_x x} , \quad (18b)$$

$$H_{y1} = -A_1 s_{y1} s_{z1} \sin(s_{y1}y) \cos(s_{z1}z) e^{-j\beta_x x} , \quad (18c)$$

$$E_{z1} = 0 , \quad (18d)$$

$$E_{x1} = j\omega\mu_1 A_1 s_{y1} \sin(s_{y1}y) \sin(s_{z1}z) e^{-j\beta_x x} , \quad (18e)$$

$$E_{y1} = \beta_x \omega\mu_1 A_1 \cos(s_{y1}y) \sin(s_{z1}z) e^{-j\beta_x x} . \quad (18f)$$

An additional boundary condition is

$$E_x = E_z = 0 \text{ at } y = a .$$

$$\text{Hence, } s_{y1}a = n\pi \Rightarrow s_{y1} = \frac{n\pi}{a} \quad (19)$$

where n is a positive integer different from zero.

A suitable Hertz function for medium 2 that satisfies the boundary conditions

$$E_x = E_z = 0 \text{ at } y = 0 \text{ and } 0 < y < +\infty ,$$

$$E_x = E_y = 0 \text{ at } z = b$$

$$\text{is } \Pi_2 = A_2 \cos(s_{y2}y) \sin[s_{z2}(z - b)] e^{-j\beta_x x} . \quad (20)$$

Introducing (20) into (3)

$$H_{z2} = A_2 (k_2^2 - s_{z2}^2) \cos(s_{y2}y) \sin[s_{z2}(z - b)] e^{-j\beta_x x} , \quad (21a)$$

$$H_{x2} = -j\beta_x A_2 s_{z2} \cos(s_{y2}y) \cos[s_{z2}(z - b)] e^{-j\beta_x x} , \quad (21b)$$

$$H_{y2} = -A_2 s_{y2} s_{z2} \sin(s_{y2}y) \cos[s_{z2}(z - b)] e^{-j\beta_x x} , \quad (21c)$$

$$E_{z1} = 0 , \quad (21d)$$

$$E_{x2} = j\omega\mu_2 A_2 s_{y2} \sin(s_{y2}y) \sin[s_{z2}(z - b)] e^{-j\beta_x x} , \quad (21e)$$

$$E_{y2} = \beta_x \omega\mu_2 A_2 \cos(s_{y2}y) \sin[s_{z2}(z - b)] e^{-j\beta_x x} . \quad (21f)$$

An additional boundary condition is

$$E_x = E_z = 0 \text{ at } y = a .$$

$$\text{Hence, } s_{y2}a = n\pi \Rightarrow s_{y2} = \frac{n\pi}{a} . \quad (22)$$

By virtue of (2.13), (2.15), (19) and (22)

$$s_{y1}^2 + s_{z1}^2 = \left(\frac{n\pi}{a}\right)^2 + s_{z1}^2 = s_1^2 = k_1^2 - \beta_x^2 \Rightarrow s_{z1} = +\sqrt{k_1^2 - \left(\frac{n\pi}{a}\right)^2 - \beta_x^2}, \quad (23)$$

$$s_{y2}^2 + s_{z2}^2 = \left(\frac{n\pi}{a}\right)^2 + s_{z2}^2 = s_2^2 = k_2^2 - \beta_x^2 \Rightarrow s_{z2} = +\sqrt{k_2^2 - \left(\frac{n\pi}{a}\right)^2 - \beta_x^2}. \quad (24)$$

Choosing the negative square roots would have no effect on the results.

The tangential components of  $\vec{E}$  and  $\vec{H}$  are continuous across the interface of two media. Furthermore, it was shown that  $s_{y1} = s_{y2}$ .

Hence,

$$H_{x1} = H_{x2} \text{ and } H_{y1} = H_{y2} \text{ at } z = h$$

$$\Rightarrow A_1 s_{z1} \cos(s_{z1}h) = A_2 s_{z2} \cos[s_{z2}(b-h)], \quad (25)$$

$$\text{as well as } E_{x1} = E_{x2} \text{ and } E_{y1} = E_{y2} \text{ at } z = h$$

$$\Rightarrow \mu_1 A_1 \sin(s_{z1}h) = -\mu_2 A_2 \sin[s_{z2}(b-h)]. \quad (26)$$

Note that (26) and (25) would have resulted in a set of contradictory equations, if  $\vec{\Pi}$  were chosen in any direction other than the z-direction.

Dividing (26) by (25) and multiplying both sides by  $j\omega$  yields

$$\frac{j\omega\mu_1 \tan(s_{z1}h)}{s_{z1}} = -\frac{j\omega\mu_2 \tan[s_{z2}(b-h)]}{s_{z2}} \quad (27)$$

or by virtue of (23) and (24)

$$\begin{aligned} & \frac{j\omega\mu_1}{\sqrt{k_1^2 - \left(\frac{n\pi}{a}\right)^2 - \beta_x^2}} \tan\left[h\sqrt{k_1^2 - \left(\frac{n\pi}{a}\right)^2 - \beta_x^2}\right] \\ &= -\frac{j\omega\mu_2}{\sqrt{k_2^2 - \left(\frac{n\pi}{a}\right)^2 - \beta_x^2}} \tan\left[(b-h)\sqrt{k_2^2 - \left(\frac{n\pi}{a}\right)^2 - \beta_x^2}\right]. \end{aligned} \quad (28)$$

This dispersion equation is transcendental and can therefore only be solved numerically for  $\beta_x$ .

Letting  $h = 0$  in (15), results in

$$\beta_x = \sqrt{k_2^2 - \left(\frac{n\pi}{a}\right)^2 - \left(\frac{m\pi}{b}\right)^2}, \text{ the dispersion equation of the } TM_{nm} \text{ empty}$$

waveguide modes.

The dispersion equation for the  $TM_{nm}$  modes of the homogeneously filled waveguide is obtained by letting  $h=b$  in (28).

### 6.3.5 On the Relation between Partially Filled Rectangular Waveguide Modes and Plane Surface Waves

Compare the dispersion equations for plane surface waves, both E-type (3.12) and H-type (3.23) with those of the waves in a partially filled waveguide (14) and (27), respectively.

Dispersion equation for E-type plane surface wave modes:

$$\frac{s_{z1}}{\sigma_1 + j\omega\epsilon_1} \tan(s_{z1}h) = \frac{js_{z2}}{\sigma_2 + j\omega\epsilon_2} \quad (3.12)$$

Dispersion equation for E-type partially filled waveguide modes:

$$\frac{s_{z1}}{\sigma_1 + j\omega\epsilon_1} \tan(s_{z1}h) = -\frac{s_{z2}}{\sigma_2 + j\omega\epsilon_2} \tan[s_{z2}(b-h)] \quad (14)$$

Dispersion equation for H-type plane surface wave modes:

$$\frac{j\omega\mu_1}{s_{z1}} \tan(s_{z1}h) = -\frac{j\omega\mu_2}{js_{z2}} \quad (3.23)$$

Dispersion equation for H-type partially filled waveguide modes:

$$\frac{j\omega\mu_1}{s_{z1}} \tan(s_{z1}h) = -\frac{j\omega\mu_2}{s_{z2}} \tan[s_{z2}(b-h)] \quad (27)$$

The only significant difference between them is a factor  $\tan[s_{z2}(b-h)]$  on the right hand side of the waveguide equations, which is replaced by  $-j$  for plane surface waves.

However, one can show that

$$\lim_{\substack{(b-h)\alpha_{z2} \rightarrow +\infty \\ (b-h)\beta_{z2} \rightarrow 0}} \tan[s_{z2}(b-h)] = -j \quad (29)$$

where  $s_{z2} = \beta_{z2} - j\alpha_{z2}$ .

The proof is as follows:

$$\begin{aligned} \lim_{\substack{(b-h)\alpha_{z2} \rightarrow +\infty \\ (b-h)\beta_{z2} \rightarrow 0}} \tan[(b-h)s_{z2}] &= \lim_{\substack{(b-h)\alpha_{z2} \rightarrow +\infty \\ (b-h)\beta_{z2} \rightarrow 0}} \tan[(b-h)(\beta_{z2} - j\alpha_{z2})] \\ &= \lim_{\substack{(b-h)\alpha_{z2} \rightarrow +\infty \\ (b-h)\beta_{z2} \rightarrow 0}} \frac{\tan[(b-h)\beta_{z2}] - \tan[j(b-h)\alpha_{z2}]}{1 + \tan[(b-h)\beta_{z2}] \cdot \tan[j(b-h)\alpha_{z2}]} \quad [8, p. 15] \\ &= \lim_{\substack{(b-h)\alpha_{z2} \rightarrow +\infty \\ (b-h)\beta_{z2} \rightarrow 0}} \frac{\tan[(b-h)\beta_{z2}] - j \cdot \tanh[(b-h)\alpha_{z2}]}{1 + j \cdot \tan[(b-h)\beta_{z2}] \cdot \tanh[(b-h)\alpha_{z2}]} \quad [8, p. 31] \\ &= -j \quad [8, p. 29] \end{aligned}$$

It is possible that the requirement  $(b-h)\alpha_{z2} \rightarrow +\infty$ , is not met by thin samples and/or samples with low values for their permittivity and permeability (see also Section 3.4.5). The requirement  $(b-h)\beta_{z2} \rightarrow 0$  may cause problems for sample materials with extremely high losses, because  $\beta_{z2}$  becomes highly negative (see Fig. 3.8). Although the factor  $(b-h)$  gives an additional degree of freedom, it should not be chosen too small though. In practice, both requirements are usually met even by surface wave absorbing materials, as is demonstrated by Example 3.

If both requirements are met, the phase constants of the partially filled waveguide modes will differ from those of the plane surface wave modes by a known constant term only.

Namely, in view of (3.8a), (3.19a), (11) and (24)

$$\beta_{xS} \Big|_{\substack{(b-h)\alpha_{z2} \rightarrow +\infty \\ (b-h)\beta_{z2} \rightarrow 0}} = \sqrt{\beta_{xW}^2 \Big|_{\substack{(b-h)\alpha_{z2} \rightarrow +\infty \\ (b-h)\beta_{z2} \rightarrow 0}} + \left(\frac{n\pi}{a}\right)^2} \quad (30)$$

where  $\beta_S$  is the phase constant of a proper surface wave mode and  $\beta_W$  the phase constant of the corresponding partially filled waveguide mode.

## The Plane Surface Wave Simulator Cell: Example 1

### Constants:

$$c_0 := 299792458 \cdot \frac{\text{m}}{\text{sec}} \quad \mu_0 := 4 \cdot \pi \cdot 10^{-7} \cdot \frac{\text{henry}}{\text{m}} \quad \epsilon_0 := \frac{1}{c_0^2 \cdot \mu_0} \quad \epsilon_0 = 8.854 \cdot 10^{-12} \cdot \frac{\text{farad}}{\text{m}}$$

### Enter the material parameters:

$$\sigma_1 := 0 \cdot \frac{\text{siemens}}{\text{m}} \quad \epsilon_{r1} := 2.33 - 0.001j \quad \mu_{r1} := 1 - 0j$$
$$\sigma_2 := 0 \cdot \frac{\text{siemens}}{\text{m}} \quad \epsilon_{r2} := 1 - 0j \quad \mu_{r2} := 1 - 0j$$

### Enter the frequency:

$$f := 8.5 \cdot 10^9 \cdot \text{Hz} \quad \omega := 2 \cdot \pi \cdot f \quad \omega = 5.341 \cdot 10^{10} \cdot \text{Hz} \quad \lambda_0 := \frac{c_0}{f} \quad \lambda_0 = 0.035 \cdot \text{m}$$

### Enter the thickness of the coating:

$$h := 0.00615 \cdot \text{m}$$

### Complex wave numbers:

$$\epsilon_1 := \epsilon_{r1} \cdot \epsilon_0 \quad \epsilon_2 := \epsilon_{r2} \cdot \epsilon_0$$

$$\mu_1 := \mu_{r1} \cdot \mu_0 \quad \mu_2 := \mu_{r2} \cdot \mu_0$$

$$k_0 := \omega \sqrt{\epsilon_0 \cdot \mu_0} \quad k_0 = 178.147 \cdot \frac{\text{rad}}{\text{m}}$$

$$k_1 := \sqrt{-j \cdot \omega \mu_1 \cdot (\sigma_1 + j \cdot \omega \epsilon_1)} \quad k_1 = 271.929 - 0.058j \cdot \frac{\text{rad}}{\text{m}}$$

$$k_2 := \sqrt{-j \cdot \omega \mu_2 \cdot (\sigma_2 + j \cdot \omega \epsilon_2)} \quad k_2 = 178.147 \cdot \frac{\text{rad}}{\text{m}}$$

( $k_2$  must be smaller than  $k_1$ !)

E-type proper surface wave modes:

$$F_{ES}(\beta_x) := \frac{\sqrt{k_1^2 - \beta_x^2}}{\sigma_1 + j \cdot \omega \varepsilon_1} \cdot \tan\left(h \cdot \sqrt{k_1^2 - \beta_x^2}\right) - \frac{\operatorname{Re}\left(\sqrt{\beta_x^2 - k_2^2}\right)}{\left|\operatorname{Re}\left(\sqrt{\beta_x^2 - k_2^2}\right)\right|} \cdot \frac{\sqrt{\beta_x^2 - k_2^2}}{\sigma_2 + j \cdot \omega \varepsilon_2}$$

$$\beta_x := \frac{k_1 + k_2}{2} \quad \beta_{xES} := \operatorname{root}(F_{ES}(\beta_x), \beta_x) \quad \beta_{xES} = 214.379 - 0.036j \cdot \frac{\text{rad}}{\text{m}}$$

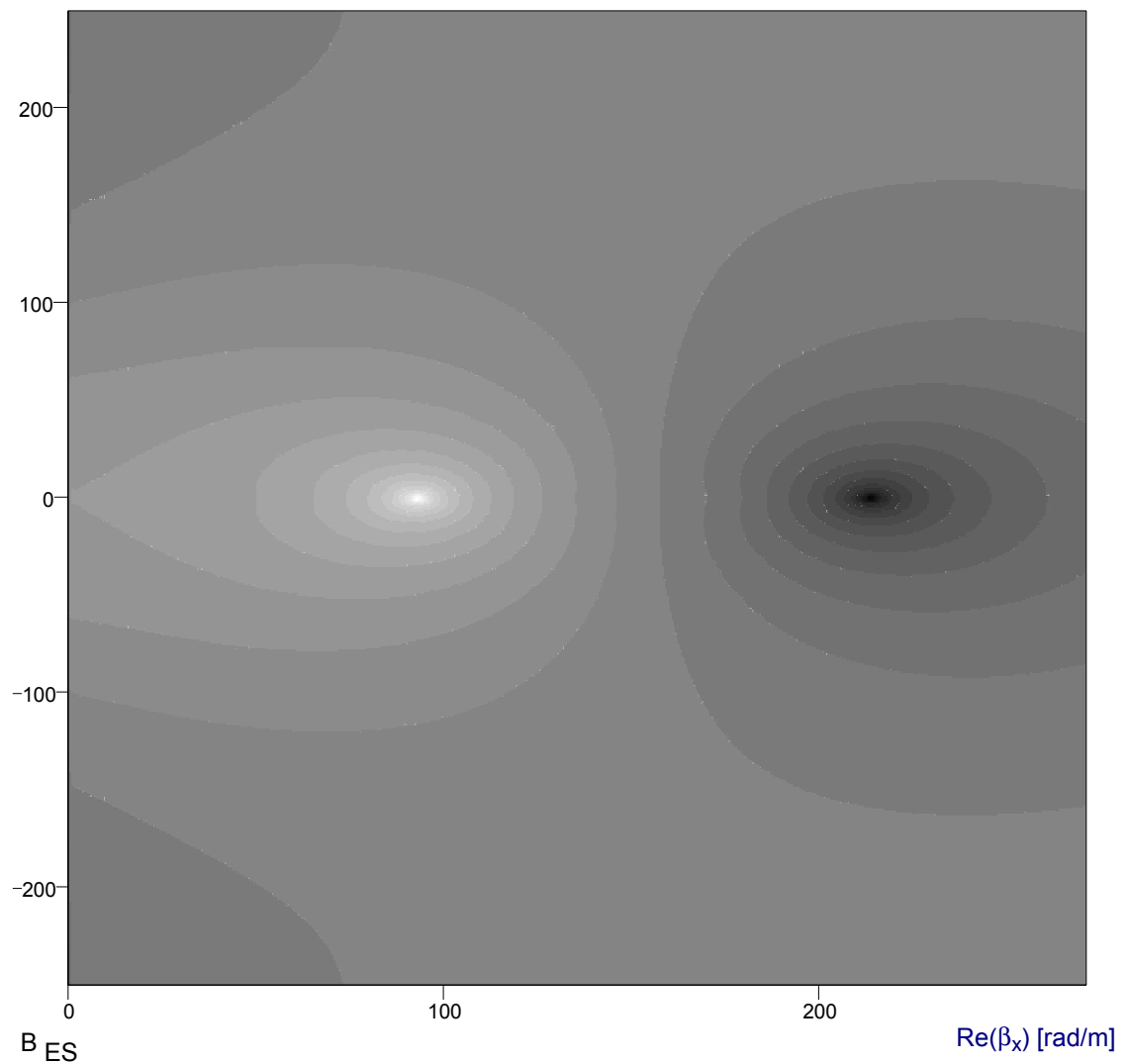
$$F_{ES}(\beta_{xES}) = 2.091 \cdot 10^{-9} - 1.441 \cdot 10^{-6} j \cdot \text{kg} \cdot \text{m}^2 \cdot \text{sec}^{-1} \cdot \text{coul}^{-2}$$

$$N := 301 \quad \text{Start}_x := 0 \cdot \frac{\text{rad}}{\text{m}} \quad \text{End}_x := \operatorname{Re}(k_1) \quad \text{Start}_y := -250 \cdot \frac{\text{rad}}{\text{m}} \quad \text{End}_y := 250 \cdot \frac{\text{rad}}{\text{m}}$$

$$x := 0, 1 \dots N \quad y := 0, 1 \dots N \quad \Delta x := \frac{\text{End}_x - \text{Start}_x}{N} \quad \Delta y := \frac{\text{End}_y - \text{Start}_y}{N}$$

$$B_{ES_{x,y}} := \log \left[ \left| F_{ES} \left[ \left( \text{Start}_x + x \cdot \Delta x \right) + \left[ j \cdot \left( \text{Start}_y + y \cdot \Delta y \right) \right] \right] \right| \cdot \frac{\text{siemens} \cdot \text{m}}{\text{m} \cdot \text{rad}} \right]$$

$\operatorname{Im}(\beta_x)$  [rad/m]



Waveguide dimensions and mode:

$$a := 0.022860 \cdot \text{m} \quad b := 0.034040 \cdot \text{m} \quad n := 1$$

E-type modes in partially filled waveguide:

$$F_{EW1}(\beta_x) := \frac{\sqrt{k_1^2 - \left(\frac{n \cdot \pi}{a}\right)^2 - \beta_x^2}}{\sigma_1 + j \cdot \omega \varepsilon_1} \cdot \tan \left[ h \cdot \sqrt{k_1^2 - \left(\frac{n \cdot \pi}{a}\right)^2 - \beta_x^2} \right]$$

$$F_{EW2}(\beta_x) := \frac{\sqrt{k_2^2 - \left(\frac{n \cdot \pi}{a}\right)^2 - \beta_x^2}}{\sigma_2 + j \cdot \omega \varepsilon_2} \cdot \tan \left[ (b - h) \cdot \sqrt{k_2^2 - \left(\frac{n \cdot \pi}{a}\right)^2 - \beta_x^2} \right]$$

$$F_{EW}(\beta_x) := F_{EW1}(\beta_x) + F_{EW2}(\beta_x)$$

$$\beta_x := \sqrt{\beta_{xES}^2 - \left(\frac{n \cdot \pi}{a}\right)^2} \quad \beta_{xEW} := \text{root}(F_{EW}(\beta_x), \beta_x) \quad \beta_{xEW} = 164.618 - 0.047j \cdot \frac{\text{rad}}{\text{m}}$$

$$F_{ES}(\beta_{xES}) = 2.091 \cdot 10^{-9} - 1.441 \cdot 10^{-6} j \cdot \text{kg} \cdot \text{m}^2 \cdot \text{sec}^{-1} \cdot \text{coul}^{-2}$$

$$\beta_{xEWc} := \sqrt{\beta_{xEW}^2 + \left(\frac{n \cdot \pi}{a}\right)^2} \quad \beta_{xEWc} = 214.442 - 0.036j \cdot \frac{\text{rad}}{\text{m}} \quad \beta_{xEW} = 164.618 - 0.047j \cdot \frac{\text{rad}}{\text{m}}$$

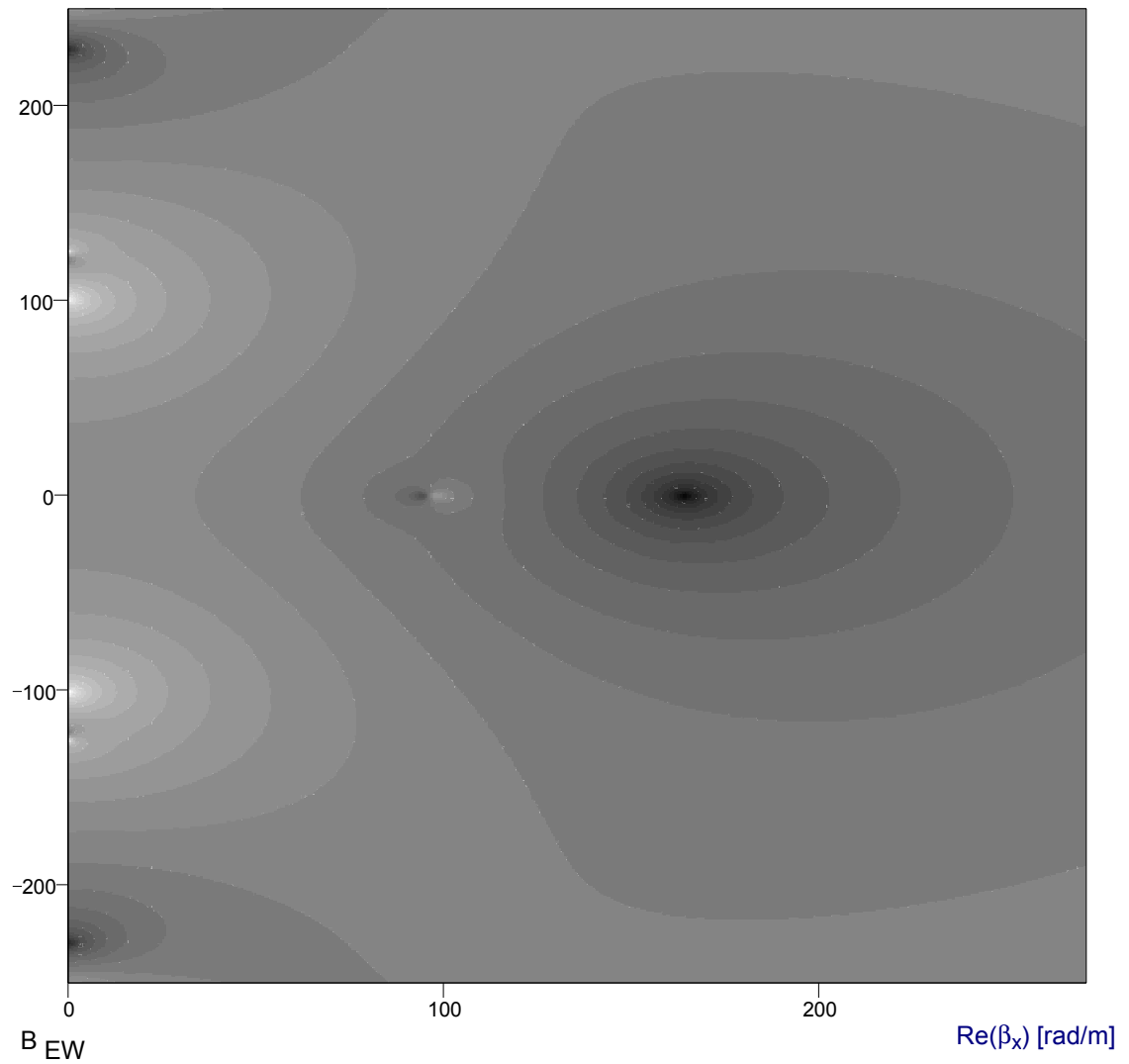
$$\frac{|\beta_{xEWc}| - |\beta_{xES}|}{|\beta_{xES}|} = 0.03 \cdot \% \quad \frac{|\beta_{xEWc}| - |\beta_{xES}|}{|k_1| - |k_2|} = 0.067 \cdot \%$$

$$N := 301 \quad \text{Start}_x := 0 \cdot \frac{\text{rad}}{\text{m}} \quad \text{End}_x := \text{Re}(k_1) \quad \text{Start}_y := -250 \cdot \frac{\text{rad}}{\text{m}} \quad \text{End}_y := 250 \cdot \frac{\text{rad}}{\text{m}}$$

$$x := 0, 1 \dots N \quad y := 0, 1 \dots N \quad \Delta x := \frac{\text{End}_x - \text{Start}_x}{N} \quad \Delta y := \frac{\text{End}_y - \text{Start}_y}{N}$$

$$B_{EW_{x,y}} := \log \left[ \left| F_{EW} \left[ (\text{Start}_x + x \cdot \Delta x) + [j \cdot (\text{Start}_y + y \cdot \Delta y)] \right] \right| \cdot \frac{\text{siemens} \cdot \text{m}}{\text{m} \cdot \text{rad}} \right]$$

$\text{Im}(\beta_x)$  [rad/m]



## The Plane Surface Wave Simulator Cell: Example 2

### Constants:

$$c_0 := 299792458 \cdot \frac{\text{m}}{\text{sec}} \quad \mu_0 := 4 \cdot \pi \cdot 10^{-7} \cdot \frac{\text{henry}}{\text{m}} \quad \varepsilon_0 := \frac{1}{c_0^2 \cdot \mu_0} \quad \varepsilon_0 = 8.854 \cdot 10^{-12} \cdot \frac{\text{farad}}{\text{m}}$$

### Enter the material parameters:

$$\sigma_1 := 0 \cdot \frac{\text{siemens}}{\text{m}} \quad \varepsilon_{r1} := 2.33 - 0.001j \quad \mu_{r1} := 1 - 0j$$

$$\sigma_2 := 0 \cdot \frac{\text{siemens}}{\text{m}} \quad \varepsilon_{r2} := 1 - 0j \quad \mu_{r2} := 1 - 0j$$

### Enter the frequency:

$$f := 8.5 \cdot 10^9 \cdot \text{Hz} \quad \omega := 2 \cdot \pi \cdot f \quad \omega = 5.341 \cdot 10^{10} \cdot \text{Hz} \quad \lambda_0 := \frac{c_0}{f} \quad \lambda_0 = 0.035 \cdot \text{m}$$

### Enter the thickness of the coating:

$$h := 0.00325 \cdot \text{m}$$

### Complex wave numbers:

$$\varepsilon_1 := \varepsilon_{r1} \cdot \varepsilon_0 \quad \varepsilon_2 := \varepsilon_{r2} \cdot \varepsilon_0$$

$$\mu_1 := \mu_{r1} \cdot \mu_0 \quad \mu_2 := \mu_{r2} \cdot \mu_0$$

$$k_0 := \omega \sqrt{\varepsilon_0 \cdot \mu_0} \quad k_0 = 178.147 \cdot \frac{\text{rad}}{\text{m}}$$

$$k_1 := \sqrt{-j \cdot \omega \mu_1 \cdot (\sigma_1 + j \cdot \omega \varepsilon_1)} \quad k_1 = 271.929 - 0.058j \cdot \frac{\text{rad}}{\text{m}}$$

$$k_2 := \sqrt{-j \cdot \omega \mu_2 \cdot (\sigma_2 + j \cdot \omega \varepsilon_2)} \quad k_2 = 178.147 \cdot \frac{\text{rad}}{\text{m}}$$

( $k_2$  must be smaller than  $k_1$ !)

E-type proper surface wave modes:

$$F_{ES}(\beta_x) := \frac{\sqrt{k_1^2 - \beta_x^2}}{\sigma_1 + j \cdot \omega \epsilon_1} \cdot \tan\left(h \cdot \sqrt{k_1^2 - \beta_x^2}\right) - \frac{\operatorname{Re}\left(\sqrt{\beta_x^2 - k_2^2}\right)}{\left|\operatorname{Re}\left(\sqrt{\beta_x^2 - k_2^2}\right)\right|} \cdot \frac{\sqrt{\beta_x^2 - k_2^2}}{\sigma_2 + j \cdot \omega \epsilon_2}$$

$$\beta_x := \frac{k_1 + k_2}{2} \quad \beta_{xES} := \operatorname{root}(F_{ES}(\beta_x), \beta_x) \quad \beta_{xES} = 188.666 - 0.009j \cdot \frac{\text{rad}}{\text{m}}$$

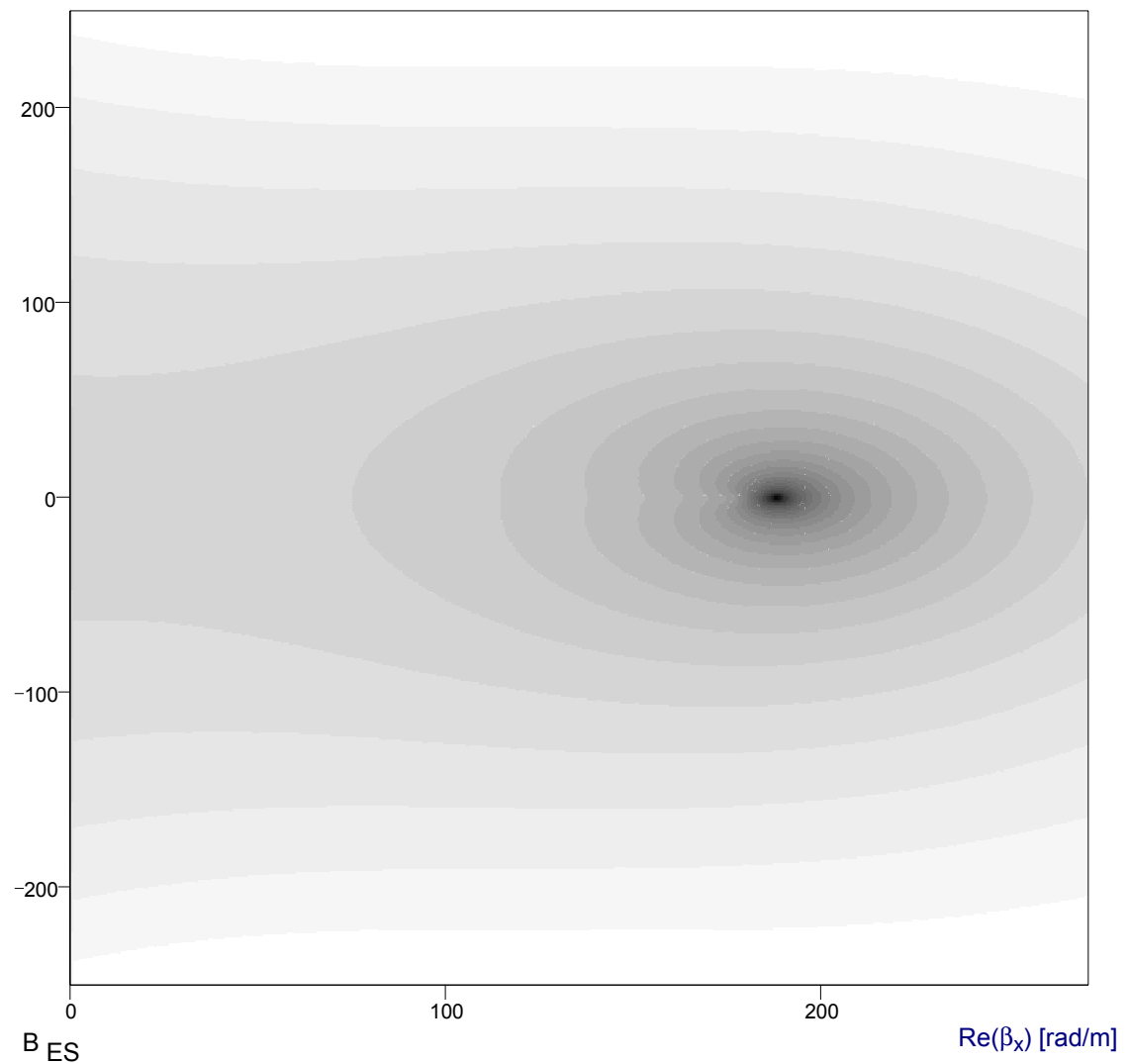
$$F_{ES}(\beta_{xES}) = -4.649 \cdot 10^{-6} + 9.477 \cdot 10^{-4} j \cdot \text{kg} \cdot \text{m}^2 \cdot \text{sec}^{-1} \cdot \text{coul}^{-2}$$

$$N := 301 \quad \text{Start}_x := 0 \cdot \frac{\text{rad}}{\text{m}} \quad \text{End}_x := \operatorname{Re}(k_1) \quad \text{Start}_y := -250 \cdot \frac{\text{rad}}{\text{m}} \quad \text{End}_y := 250 \cdot \frac{\text{rad}}{\text{m}}$$

$$x := 0, 1 \dots N \quad y := 0, 1 \dots N \quad \Delta x := \frac{\text{End}_x - \text{Start}_x}{N} \quad \Delta y := \frac{\text{End}_y - \text{Start}_y}{N}$$

$$B_{ES_{x,y}} := \log\left[\left|F_{ES}\left(\left(\text{Start}_x + x \cdot \Delta x\right) + \left[j \cdot \left(\text{Start}_y + y \cdot \Delta y\right)\right]\right)\right| \cdot \frac{\text{siemens} \cdot \text{m}}{\text{m} \cdot \text{rad}}\right]$$

$\operatorname{Im}(\beta_x)$  [rad/m]



Waveguide dimensions and mode:

$$a := 0.022860 \cdot \text{m} \quad b := 0.034040 \cdot \text{m} \quad n := 1$$

E-type modes in partially filled waveguide:

$$F_{EW1}(\beta_x) := \frac{\sqrt{k_1^2 - \left(\frac{n \cdot \pi}{a}\right)^2 - \beta_x^2}}{\sigma_1 + j \cdot \omega \varepsilon_1} \cdot \tan \left[ h \cdot \sqrt{k_1^2 - \left(\frac{n \cdot \pi}{a}\right)^2 - \beta_x^2} \right]$$

$$F_{EW2}(\beta_x) := \frac{\sqrt{k_2^2 - \left(\frac{n \cdot \pi}{a}\right)^2 - \beta_x^2}}{\sigma_2 + j \cdot \omega \varepsilon_2} \cdot \tan \left[ (b - h) \cdot \sqrt{k_2^2 - \left(\frac{n \cdot \pi}{a}\right)^2 - \beta_x^2} \right]$$

$$F_{EW}(\beta_x) := F_{EW1}(\beta_x) + F_{EW2}(\beta_x)$$

$$\beta_x := \sqrt{\beta_{xES}^2 - \left(\frac{n \cdot \pi}{a}\right)^2} \quad \beta_{xEW} := \text{root}(F_{EW}(\beta_x), \beta_x) \quad \beta_{xEW} = 130.216 - 0.012j \cdot \frac{\text{rad}}{\text{m}}$$

$$F_{ES}(\beta_{xES}) = -4.649 \cdot 10^{-6} + 9.477 \cdot 10^{-4} j \cdot \text{kg} \cdot \text{m}^2 \cdot \text{sec}^{-1} \cdot \text{coul}^{-2}$$

$$\beta_{xEWc} := \sqrt{\beta_{xEW}^2 + \left(\frac{n \cdot \pi}{a}\right)^2} \quad \beta_{xEWc} = 189.321 - 0.008j \cdot \frac{\text{rad}}{\text{m}} \quad \beta_{xEW} = 130.216 - 0.012j \cdot \frac{\text{rad}}{\text{m}}$$

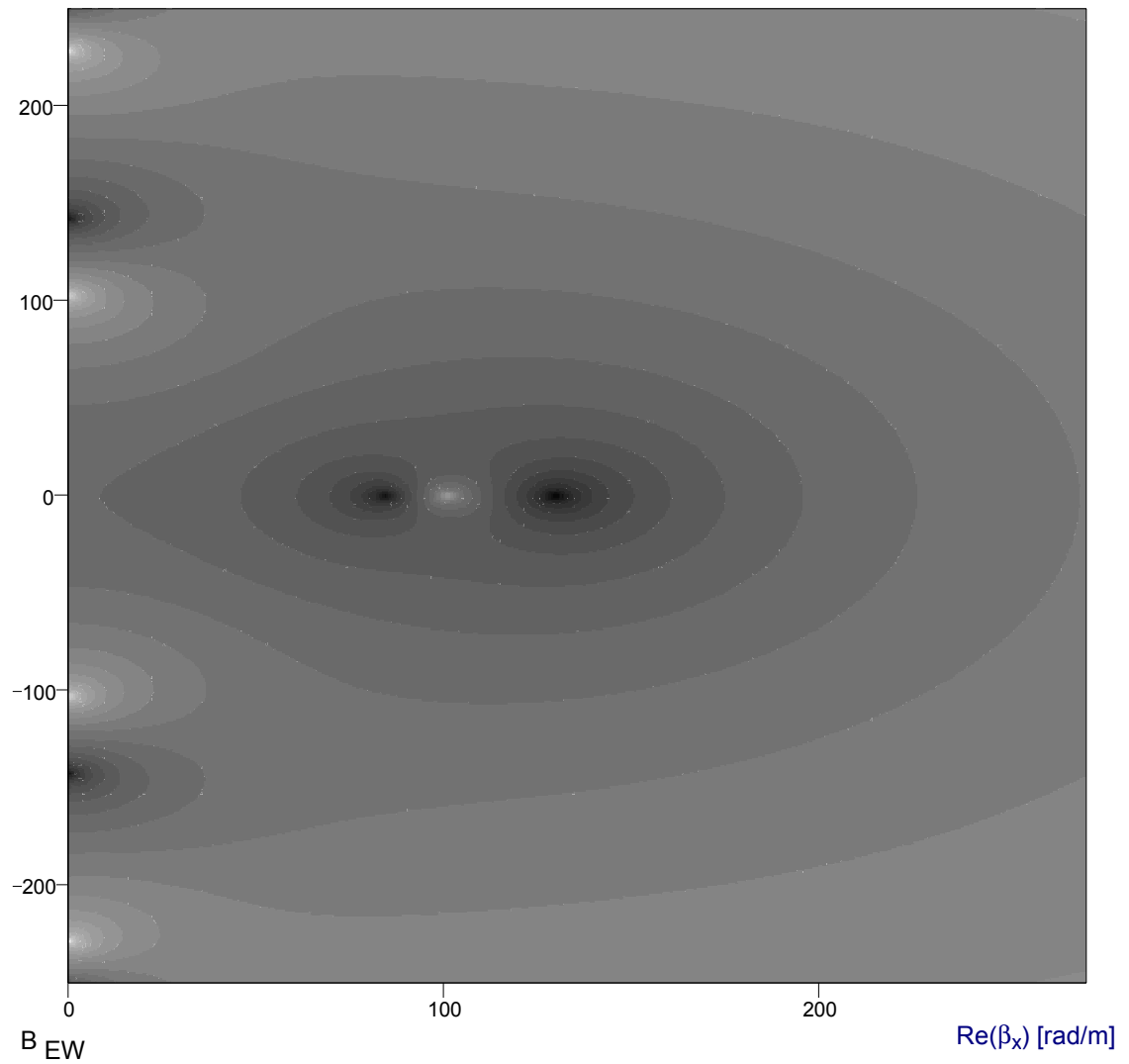
$$\frac{|\beta_{xEWc}| - |\beta_{xES}|}{|\beta_{xES}|} = 0.347 \cdot \% \quad \frac{|\beta_{xEWc}| - |\beta_{xES}|}{|k_1| - |k_2|} = 0.699 \cdot \%$$

$$N := 301 \quad \text{Start}_x := 0 \cdot \frac{\text{rad}}{\text{m}} \quad \text{End}_x := \text{Re}(k_1) \quad \text{Start}_y := -250 \cdot \frac{\text{rad}}{\text{m}} \quad \text{End}_y := 250 \cdot \frac{\text{rad}}{\text{m}}$$

$$x := 0, 1 \dots N \quad y := 0, 1 \dots N \quad \Delta x := \frac{\text{End}_x - \text{Start}_x}{N} \quad \Delta y := \frac{\text{End}_y - \text{Start}_y}{N}$$

$$B_{EW_{x,y}} := \log \left[ \left| F_{EW} \left[ (\text{Start}_x + x \cdot \Delta x) + [j \cdot (\text{Start}_y + y \cdot \Delta y)] \right] \right| \cdot \frac{\text{siemens} \cdot \text{m}}{\text{m} \cdot \text{rad}} \right]$$

$\text{Im}(\beta_x)$  [rad/m]



## The Plane Surface Wave Simulator Cell: Example 3

### Constants:

$$c_0 := 299792458 \cdot \frac{\text{m}}{\text{sec}} \quad \mu_0 := 4 \cdot \pi \cdot 10^{-7} \cdot \frac{\text{henry}}{\text{m}} \quad \varepsilon_0 := \frac{1}{c_0^2 \cdot \mu_0} \quad \varepsilon_0 = 8.854 \cdot 10^{-12} \cdot \frac{\text{farad}}{\text{m}}$$

### Enter the material parameters:

$$\sigma_1 := 0 \cdot \frac{\text{siemens}}{\text{m}} \quad \varepsilon_{r1} := 7.4 - 0.15j \quad \mu_{r1} := 1.4 - 0.48j$$

$$\sigma_2 := 0 \cdot \frac{\text{siemens}}{\text{m}} \quad \varepsilon_{r2} := 1 - 0j \quad \mu_{r2} := 1 - 0j$$

### Enter the frequency:

$$f := 8.6 \cdot 10^9 \cdot \text{Hz} \quad \omega := 2 \cdot \pi \cdot f \quad \omega = 5.404 \cdot 10^{10} \cdot \text{Hz} \quad \lambda_0 := \frac{c_0}{f} \quad \lambda_0 = 0.035 \cdot \text{m}$$

### Enter the thickness of the coating:

$$h := 0.00075 \cdot \text{m}$$

### Complex wave numbers:

$$\varepsilon_1 := \varepsilon_{r1} \cdot \varepsilon_0 \quad \varepsilon_2 := \varepsilon_{r2} \cdot \varepsilon_0$$

$$\mu_1 := \mu_{r1} \cdot \mu_0 \quad \mu_2 := \mu_{r2} \cdot \mu_0$$

$$k_0 := \omega \sqrt{\varepsilon_0 \cdot \mu_0} \quad k_0 = 180.243 \cdot \frac{\text{rad}}{\text{m}}$$

$$k_1 := \sqrt{-j \cdot \omega \mu_1 \cdot (\sigma_1 + j \cdot \omega \varepsilon_1)} \quad k_1 = 587.412 - 104.031j \cdot \frac{\text{rad}}{\text{m}}$$

(k<sub>2</sub> must be smaller than k<sub>1</sub>!)

$$k_2 := \sqrt{-j \cdot \omega \mu_2 \cdot (\sigma_2 + j \cdot \omega \varepsilon_2)} \quad k_2 = 180.243 \cdot \frac{\text{rad}}{\text{m}}$$

E-type proper surface wave modes:

$$F_{ES}(\beta_x) := \frac{\sqrt{k_1^2 - \beta_x^2}}{\sigma_1 + j \cdot \omega \varepsilon_1} \cdot \tan\left(h \cdot \sqrt{k_1^2 - \beta_x^2}\right) - \frac{\operatorname{Re}\left(\sqrt{\beta_x^2 - k_2^2}\right)}{\left|\operatorname{Re}\left(\sqrt{\beta_x^2 - k_2^2}\right)\right|} \cdot \frac{\sqrt{\beta_x^2 - k_2^2}}{\sigma_2 + j \cdot \omega \varepsilon_2}$$

$$\beta_x := \frac{k_1 + k_2}{2} \quad \beta_{xES} := \operatorname{root}(F_{ES}(\beta_x), \beta_x) \quad \beta_{xES} = 182.647 - 2.328j \cdot \frac{\operatorname{rad}}{\operatorname{m}}$$

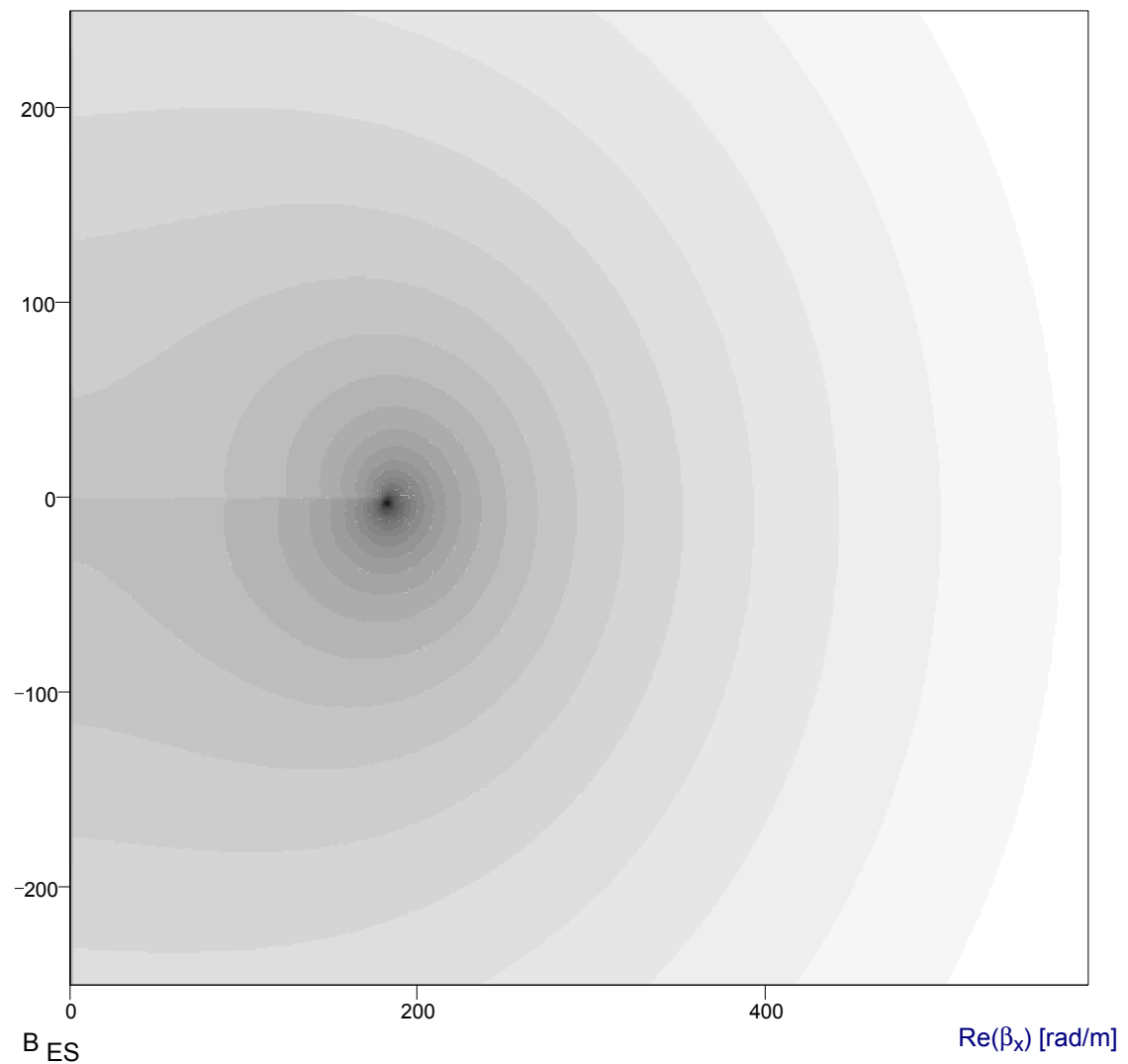
$$F_{ES}(\beta_{xES}) = -2.203 \cdot 10^{-4} + 6.845 \cdot 10^{-4} j \cdot \operatorname{kg} \cdot \operatorname{m}^2 \cdot \operatorname{sec}^{-1} \cdot \operatorname{coul}^{-2}$$

$$N := 301 \quad \operatorname{Start}_x := 0 \cdot \frac{\operatorname{rad}}{\operatorname{m}} \quad \operatorname{End}_x := \operatorname{Re}(k_1) \quad \operatorname{Start}_y := -250 \cdot \frac{\operatorname{rad}}{\operatorname{m}} \quad \operatorname{End}_y := 250 \cdot \frac{\operatorname{rad}}{\operatorname{m}}$$

$$x := 0, 1 \dots N \quad y := 0, 1 \dots N \quad \Delta x := \frac{\operatorname{End}_x - \operatorname{Start}_x}{N} \quad \Delta y := \frac{\operatorname{End}_y - \operatorname{Start}_y}{N}$$

$$B_{ES_{x,y}} := \log\left[\left|F_{ES}\left(\left(\operatorname{Start}_x + x \cdot \Delta x\right) + \left[j \cdot \left(\operatorname{Start}_y + y \cdot \Delta y\right)\right]\right)\right| \cdot \frac{\operatorname{siemens}}{\operatorname{m}} \cdot \frac{\operatorname{m}}{\operatorname{rad}}\right]$$

$\operatorname{Im}(\beta_x)$  [rad/m]



Waveguide dimensions and mode:

$$a := 0.022860 \cdot \text{m} \quad b := 0.034040 \cdot \text{m} \quad n := 1$$

E-type modes in partially filled waveguide:

$$F_{EW1}(\beta_x) := \frac{\sqrt{k_1^2 - \left(\frac{n \cdot \pi}{a}\right)^2 - \beta_x^2}}{\sigma_1 + j \cdot \omega \varepsilon_1} \cdot \tan \left[ h \cdot \sqrt{k_1^2 - \left(\frac{n \cdot \pi}{a}\right)^2 - \beta_x^2} \right]$$

$$F_{EW2}(\beta_x) := \frac{\sqrt{k_2^2 - \left(\frac{n \cdot \pi}{a}\right)^2 - \beta_x^2}}{\sigma_2 + j \cdot \omega \varepsilon_2} \cdot \tan \left[ (b - h) \cdot \sqrt{k_2^2 - \left(\frac{n \cdot \pi}{a}\right)^2 - \beta_x^2} \right]$$

$$F_{EW}(\beta_x) := F_{EW1}(\beta_x) + F_{EW2}(\beta_x)$$

$$\beta_x := \sqrt{\beta_{xES}^2 - \left(\frac{n \cdot \pi}{a}\right)^2} \quad \beta_{xEW} := \text{root}(F_{EW}(\beta_x), \beta_x) \quad \beta_{xEW} = 122.142 - 3.364j \cdot \frac{\text{rad}}{\text{m}}$$

$$F_{ES}(\beta_{xES}) = -2.203 \cdot 10^{-4} + 6.845 \cdot 10^{-4} j \cdot \text{kg} \cdot \text{m}^2 \cdot \text{sec}^{-1} \cdot \text{coul}^{-2}$$

$$\beta_{xEWc} := \sqrt{\beta_{xEW}^2 + \left(\frac{n \cdot \pi}{a}\right)^2} \quad \beta_{xEWc} = 183.844 - 2.235j \cdot \frac{\text{rad}}{\text{m}} \quad \beta_{xEW} = 122.142 - 3.364j \cdot \frac{\text{rad}}{\text{m}}$$

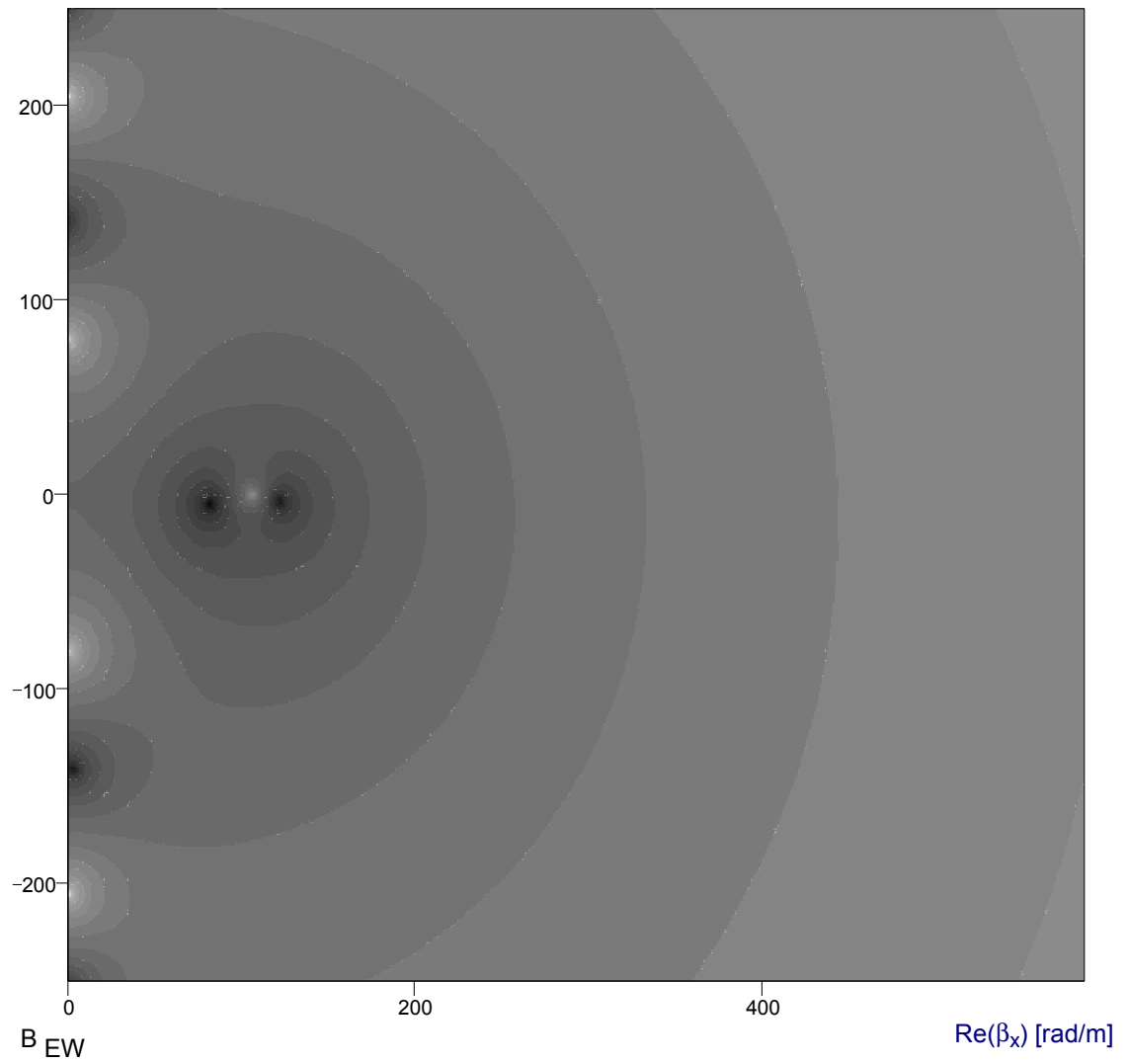
$$\frac{|\beta_{xEWc}| - |\beta_{xES}|}{|\beta_{xES}|} = 0.655 \cdot \% \quad \frac{|\beta_{xEWc}| - |\beta_{xES}|}{|k_1| - |k_2|} = 0.287 \cdot \%$$

$$N := 301 \quad \text{Start}_x := 0 \cdot \frac{\text{rad}}{\text{m}} \quad \text{End}_x := \text{Re}(k_1) \quad \text{Start}_y := -250 \cdot \frac{\text{rad}}{\text{m}} \quad \text{End}_y := 250 \cdot \frac{\text{rad}}{\text{m}}$$

$$x := 0, 1 \dots N \quad y := 0, 1 \dots N \quad \Delta x := \frac{\text{End}_x - \text{Start}_x}{N} \quad \Delta y := \frac{\text{End}_y - \text{Start}_y}{N}$$

$$B_{EW_{x,y}} := \log \left[ \left| F_{EW} \left[ (\text{Start}_x + x \cdot \Delta x) + [j \cdot (\text{Start}_y + y \cdot \Delta y)] \right] \right| \cdot \frac{\text{siemens} \cdot \text{m}}{\text{rad}} \right]$$

$\text{Im}(\beta_x)$  [rad/m]



### 6.3.6 The Plane Surface Wave Simulator Cell

A plane surface wave simulator cell (Fig. 6.4) has been designed to measure the complex phase constant of a fundamental E-mode plane surface wave mode at X-band frequencies. The experimental system can be used to measure materials up to approximately 8mm in thickness. A sample of the material under test is placed on the floor of the test cell over its entire length, 800mm for this design. The first section of the test cell, ①, is a section of standard X-band waveguide. A coax to waveguide adaptor fits to the input of the test cell. Along the length of section ①, the sample is tapered in the H-plane to provide a matched transition between the empty and partially filled waveguide sections. The transition converts the fundamental empty waveguide mode  $TE_{10}$  into a fundamental ( $n=1$ ) partially filled waveguide mode. After this transition, the waveguide height is increased to 34.04mm via a taper (section ②) on the upper horizontal wall of the waveguide. A taper from 10.16mm to 34.04 mm (the height of a WG10 S-band waveguide) is quite common in industry and will not convert a lot of fundamental mode energy into higher order modes. Section ③ will support the fundamental partially filled waveguide mode that resembles the plane surface wave. At the furthest end, the test cell is terminated with a short circuit ④. The test cell can be opened at the top. This makes fastening the test material a lot easier. However, this also implies that the waveguide has to be cut along its length. The cut is parallel with the H-plane and located in a corner of the waveguide as field intensities are at their lowest there. Also, the wall thickness of the waveguide is an odd multiple of the trapping distance of a standard WG16 X-band waveguide flange. The screws are positioned at an even multiple of this distance. Detailed engineering drawings are included at the end of this section.

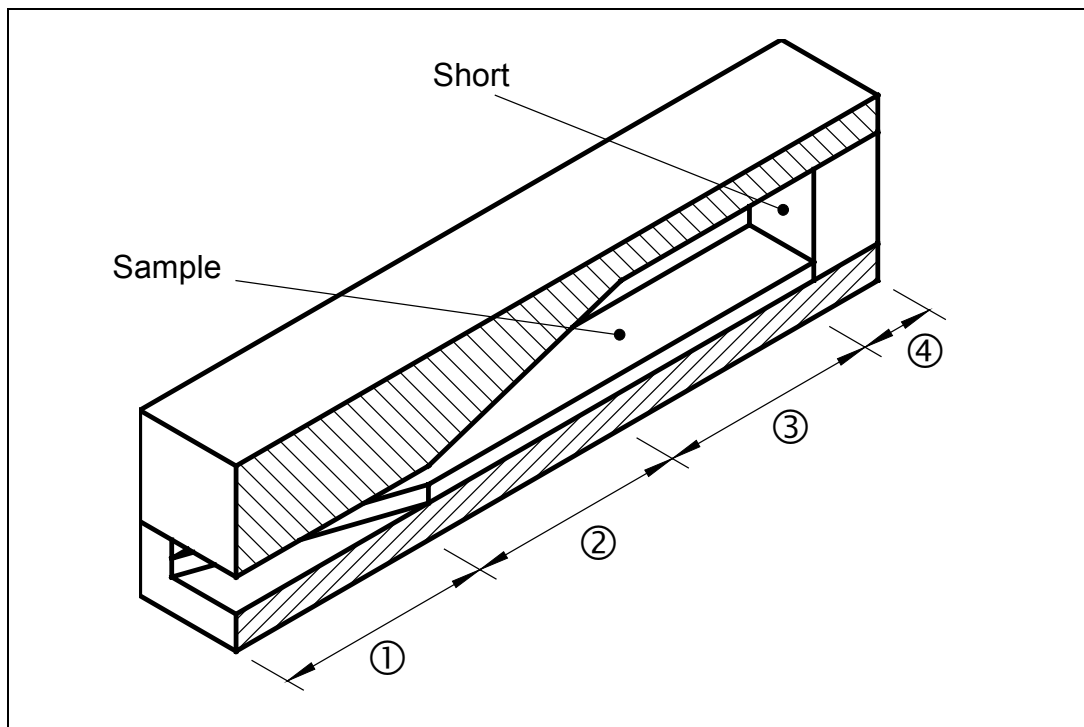


Figure 6.4: Cutaway view of the plane surface wave simulator cell (not to scale)

Two or more measurements of the input impedance  $Z_{in}$  are made the plane surface wave simulator cell terminated by a short circuit at different positions. From this, the complex propagation constant of the fundamental partially filled waveguide mode in section ③ can be obtained as follows.

The input impedance  $Z_{in}$  of a transmission line of length  $\ell$  and terminated by a short circuit is given by the following expression

$$Z_{in} = jZ_c \tan(\beta\ell) \quad (31)$$

where  $Z_c$  is the characteristic impedance of the transmission line.

Rearranging (31) for  $Z_c$  gives

$$Z_c = \frac{Z_{in}}{j \cdot \tan(\beta\ell)} = -jZ_{in} \cot(\beta\ell). \quad (32)$$

The wave impedance of a waveguide corresponds to the characteristic impedance of a transmission line. Moreover, the wave impedance is constant over the length of section ③. Hence, for two input impedance measurements made with a short circuit in two different positions:

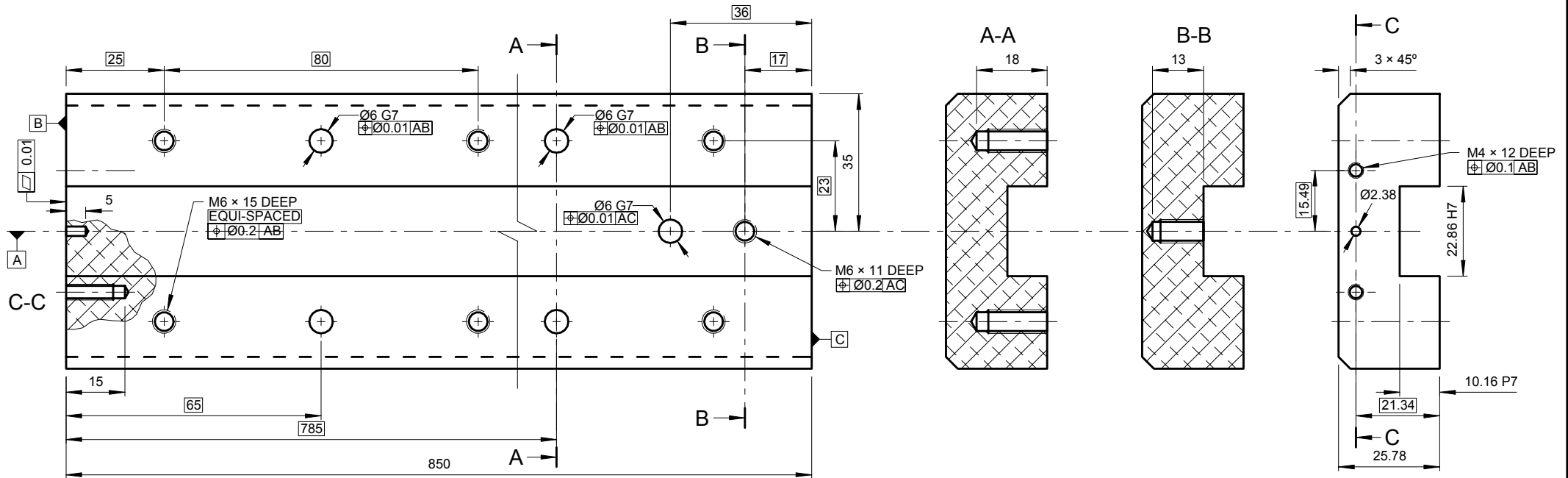
$$\begin{aligned} -jZ_{in1} \cot(\beta_m \ell_1) &= -jZ_{in2} \cot(\beta_m \ell_2) \\ \Rightarrow Z_{in1} \cot(\beta_m \ell_1) &= Z_{in2} \cot(\beta_m \ell_2) \end{aligned} \quad (33)$$

where  $\beta_m$  is the measured complex phase constant of the fundamental partially filled waveguide mode in section ③.

Equation (33) is a transcendental and can therefore only be solved numerically for  $\beta_m$ . In general, equation (33) will have more than one solution. There are two ways of finding the right solution. If the permittivity and permeability of the material under test is known from other measurements, the correct solution will be the solution closest to the theoretical value of  $\beta_s$ . However, in many cases, very little is known on the electromagnetic properties of surface wave absorbing materials. For these materials, more than two input impedance measurements are needed, resulting in additional equations similar to (33). The correct solution in this case is the solution which all equations have in common.

The input impedance data is obtained from reflection measurements made with the aid of a vector network analyser (VNA). Here, the reflection measurements are calibrated for tracking error (variations in magnitude and phase frequency response) using an additional measurement which defines the phase reference plane. The remaining two systematic errors are reduced using time domain filtering. The dimensions of the test cell ensure the time domain response of the sample is isolated from other error responses. Note that the directivity error is not only caused by leakage signals in the separation device of the VNA but is also due to residual reflection effects of test cables, adaptors and waveguide transitions between the signal separation device and the measurement plane. Source match error is particularly a problem when measuring very high or very low impedances (large mismatch at the measurement plane) [9].

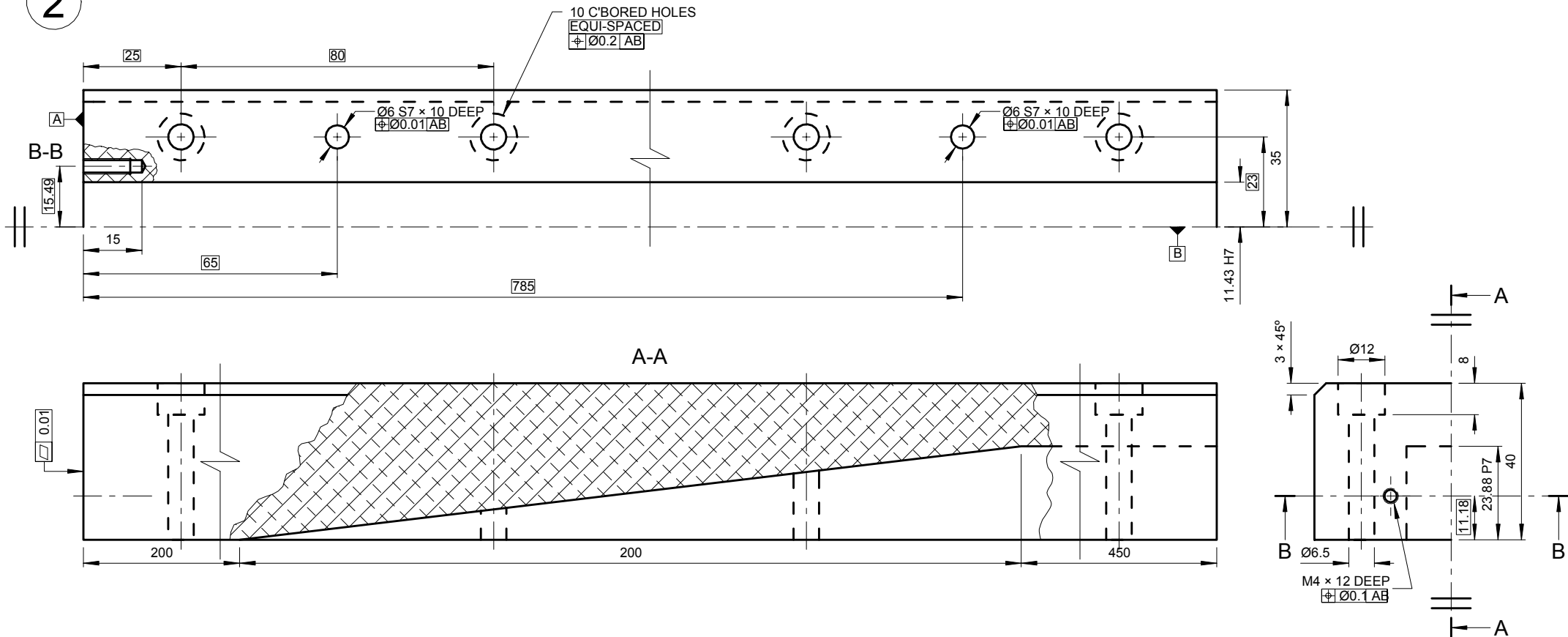
1



- MATERIAL: ALUMINIUM
- USE STAINLESS STEEL SOCKET CAP SCREWS

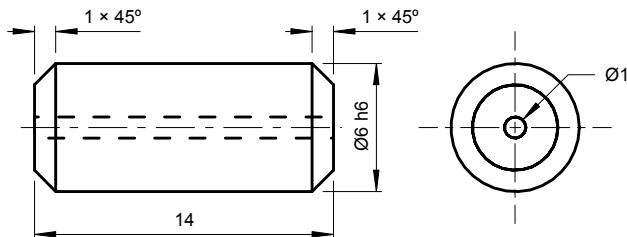
TITLE		
MEASUREMENT CELL		
THE UNIVERSITY OF HULL		
	DRAWN BY S. Y. M. R. STROOBANDT	DRAWING 1 OF 3
	APPROVED BY F. C. SMITH	ORIGINAL SCALE 1:1 ON A3
DATE 3 OCTOBER 1996	DIMENSIONS IN MILLIMETERS	

2



- MATERIAL: ALUMINIUM
- USE STAINLESS STEEL SOCKET CAP SCREWS

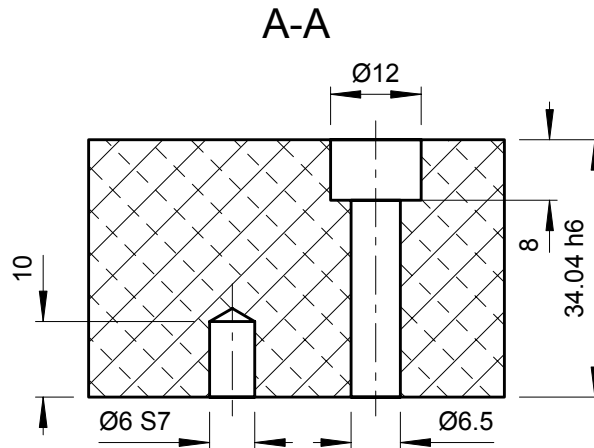
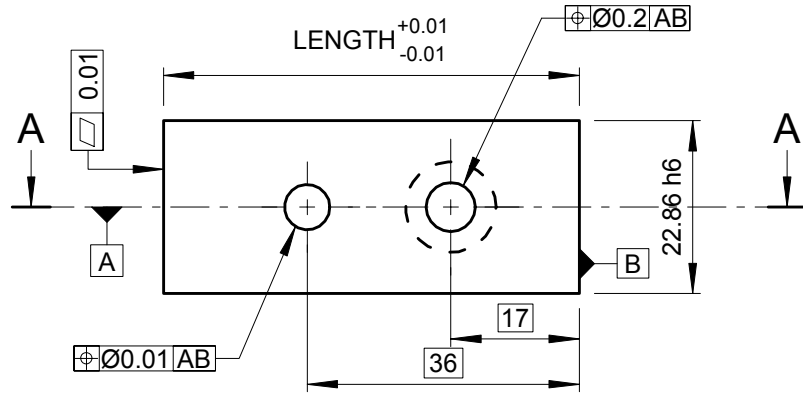
3



- ORIGINAL SCALE: 4:1 ON A3
- MATERIAL: STAINLESS STEEL

TITLE			
MEASUREMENT CELL			
THE UNIVERSITY OF HULL			
	DRAWN BY	S. Y. M. R. STROOBANDT	DRAWING
	APPROVED BY	F. C. SMITH	2 OF 3
	DATE	4 OCTOBER 1996	ORIGINAL SCALE
			DIMENSIONS IN MILLIMETERS

4 5 6



PART	LENGTH
4	250
5	55
6	50

- MATERIAL: ALUMINIUM
- USE A STAINLESS STEEL SOCKET CAP SCREW

TITLE		
<b>MEASUREMENT CELL</b>		
<b>THE UNIVERSITY OF HULL</b>		
	DRAWN BY S. Y. M. R. STROOBANDT	DRAWING 3 OF 3
	APPROVED BY F. C. SMITH	ORIGINAL SCALE 1:1 ON A4
	DATE 8 OCTOBER 1996	DIMENSIONS IN MILLIMETERS

### 6.3.7 Measurement Results

Measurements have been performed using high molecular weight polyethylene (HMW-PE). Material thicknesses of 6.15mm and 3.25mm have been used. Because polyethylene has very low losses, only results relating to phase constants have been calculated. The measurement of lossy materials is made marginally easier by the reduction in the magnitude of the source match error.

The cell has only been used to interrogate the fundamental E-type plane surface wave mode because only a probe-type coax to waveguide adaptor was available. However, the same test cell could also be used to interrogate the fundamental H-type plane surface wave mode by employing a loop-type coax to waveguide adaptor.

Results for measurements of the fundamental E-type plane surface wave mode are presented on the following pages. The tabulated quantities are:

$\beta_{S\_th}$  is the theoretical predicted value for the phase constant of the proper fundamental E-type plane surface wave; this value is obtained from equation (3.13), using measured data of  $\epsilon_r$  and  $\mu_r$ ,

$\beta_{W\_th\&c}$  is the theoretical value for the phase constant of the fundamental E-type partially filled waveguide mode (eq. (15)), corrected for horizontal confinement (eq. (30)),

$\beta_{m\&c}$  is the value for the measured phase constant of the fundamental E-type partially filled waveguide mode, obtained from  $Z_{in1}$ ,  $Z_{in2}$  and equation (33), also corrected for horizontal confinement (eq. (30)),

$$\text{relative error} = \frac{|\beta_{m\&c}| - |\beta_{S\_th}|}{|\beta_{S\_th}|}, \quad (34)$$

$$\text{nominal error} = \frac{|\beta_{m\&c}| - |\beta_{S\_th}|}{|k_1| - |k_2|}, \quad (35)$$

and finally, the relative estimated uncertainty in  $\beta_{m\&c}$  due to measurement uncertainties in  $Z_{in1}$  and  $Z_{in2}$  are given by

$$\frac{\partial \beta_{m\&c}}{\partial Z_1} \text{ and } \frac{\partial \beta_{m\&c}}{\partial Z_2}, \text{ respectively.}$$

If the measurement uncertainties  $\Delta Z_{in1}$  and  $\Delta Z_{in2}$  were known, then the total estimated uncertainty in  $\beta_{m\&c}$  could be calculated as follows

$$\Delta \beta_{m\&c} = \sqrt{\left( \frac{\partial \beta_{m\&c}}{\partial Z_{in1}} \cdot \Delta Z_{in1} \right)^2 + \left( \frac{\partial \beta_{m\&c}}{\partial Z_{in2}} \cdot \Delta Z_{in2} \right)^2}. \quad (36)$$

However, in practice, it is extremely difficult to make reasonable estimations of the measurement uncertainties  $\Delta Z_{in1}$  and  $\Delta Z_{in2}$ ; the values specified in the VNA manual are very pessimistic worst-case values and hence not realistic.

The results show good agreement between the measured and predicted values. Due to the higher impedance mismatch between the empty and partially filled sections of waveguide, an increase in ripple is seen in the data corresponding to the 6.15mm sample. However, improved tapering between the empty and partially filled sections would reduce this error. Care should also be taken when fastening the sample in the test cell. Air gaps between the sample and the bottom of the test cell can significantly affect the results.

# The Plane Surface Wave Simulator Cell

## Measurement Results for a 6.15mm Thick HMW-PE Sample

### Physical constants

$c_0$ (m/s)	299 792 458
$\mu_0$ (H/m)	1.257E-06
$\varepsilon_0$ (F/m)	8.854E-12

### Material parameters

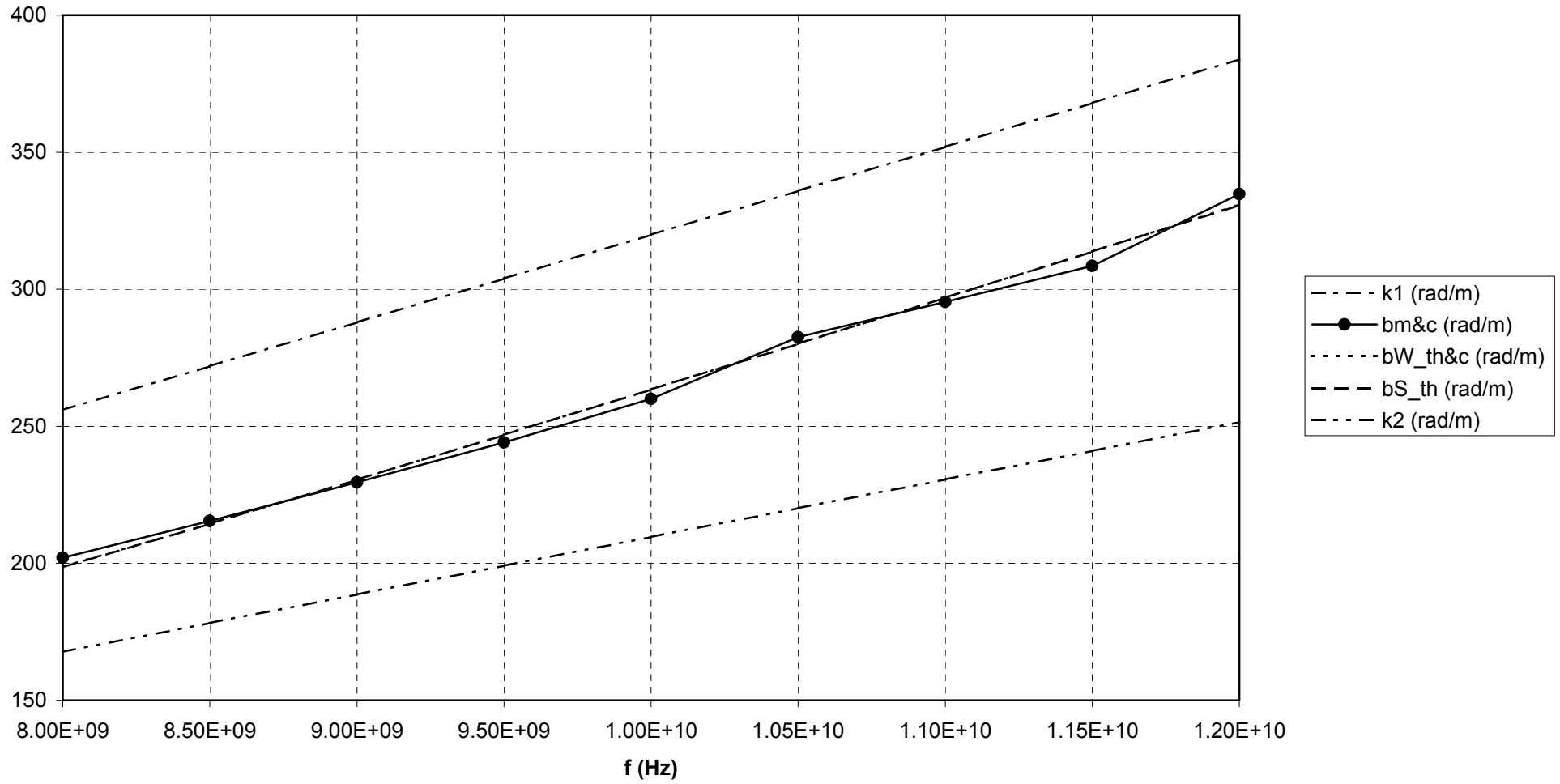
	medium 1	medium 2
$\varepsilon_r$	2.33	1.00
$\mu_r$	1.00	1.00
$\varepsilon$ (F/m)	2.063E-11	8.854E-12
$\mu$ (H/m)	1.257E-06	1.257E-06
$h$ (m)	6.000E-03	

### Results

f (Hz)	$\beta_{S\_th}$ (rad/m)	$\beta_{W\_th\&c}$ (rad/m)	$X_{in1}$ ( $\Omega$ )	$X_{in2}$ ( $\Omega$ )	$\beta_{m\&c}$ (rad/m)	rel. err.	nom. err.	$\partial\beta_{m\&c}/\partial Z_{in1}$ (rad·m <sup>-1</sup> · $\Omega^{-1}$ )	$\partial\beta_{m\&c}/\partial Z_{in2}$ (rad·m <sup>-1</sup> · $\Omega^{-1}$ )
8.00E+09	198.5	198.7	+12.4	+75.8	202.0	+1.7%	+3.9%	NC	NC
8.50E+09	214.4	214.4	+46.1	-168	215.4	+0.5%	+1.1%	3.65E-04	3.18E-03
9.00E+09	230.5	230.5	+122	-46.7	229.5	-0.4%	-1.0%	5.68E-03	1.48E-02
9.50E+09	246.9	246.9	-361	-13.3	244.1	-1.1%	-2.6%	9.61E-04	2.61E-02
1.00E+10	263.4	263.4	-102	+12.5	260.0	-1.3%	-3.1%	5.08E-03	4.12E-02
1.05E+10	280.1	280.1	-59.0	+44.9	282.6	+0.9%	+2.1%	1.75E-02	2.30E-02
1.10E+10	296.9	296.9	-32.4	+74.0	295.4	-0.5%	-1.2%	3.05E-02	1.33E-02
1.15E+10	313.8	313.8	-25.5	+196	308.5	-1.7%	-4.2%	2.71E-02	3.52E-03
1.20E+10	330.7	331.0	-34.0	+865	334.7	+1.2%	+3.0%	1.29E-02	5.06E-04

See text for more information on the tabulated quantities. NC means "Not Converging."

### HMW-PE 6.15mm



# The Plane Surface Wave Simulator Cell

## Measurement Results for a 3.25mm Thick HMW-PE Sample

### Physical constants

$c_0$ (m/s)	299 792 458
$\mu_0$ (H/m)	1.257E-06
$\epsilon_0$ (F/m)	8.854E-12

### Material parameters

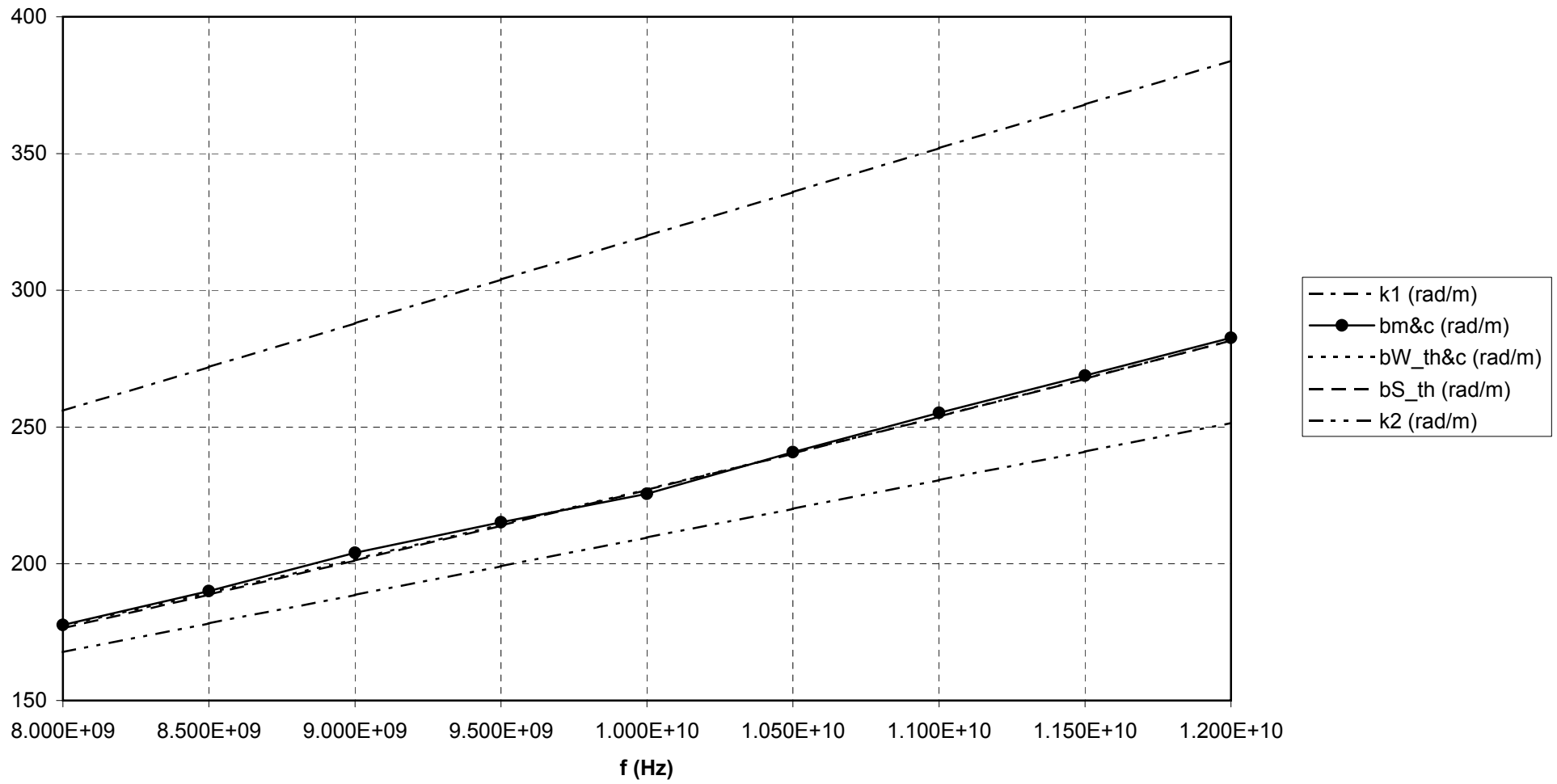
	medium 1	medium 2
$\epsilon_r$	2.33	1.00
$\mu_r$	1.00	1.00
$\epsilon$ (F/m)	2.063E-11	8.854E-12
$\mu$ (H/m)	1.257E-06	1.257E-06
$h$ (m)	3.250E-03	

### Results

f (Hz)	$\beta_{S\_th}$ (rad/m)	$\beta_{W\_th\&c}$ (rad/m)	$X_{in1}$ ( $\Omega$ )	$X_{in2}$ ( $\Omega$ )	$\beta_{m\&c}$ (rad/m)	rel. err.	nom. err.	$\partial\beta_{m\&c}/\partial Z_{in1}$ (rad·m <sup>-1</sup> · $\Omega^{-1}$ )	$\partial\beta_{m\&c}/\partial Z_{in2}$ (rad·m <sup>-1</sup> · $\Omega^{-1}$ )
8.000E+09	176.4	177.2	-2.0	+20.3	177.6	+0.7%	+1.4%	7.84E-04	7.73E-03
8.500E+09	188.7	189.3	+16.5	+44.3	190.0	+0.7%	+1.4%	NC	NC
9.000E+09	201.2	201.7	+29.9	-42.0	204.0	+1.4%	+2.9%	2.09E-02	1.49E-02
9.500E+09	213.9	214.3	+76.9	-530	215.2	+0.6%	+1.2%	4.90E-03	7.11E-04
1.000E+10	227.0	227.2	+36.5	+161	225.6	-0.6%	-1.2%	NC	NC
1.050E+10	240.2	240.4	+41.1	-132	240.8	+0.2%	+0.5%	1.69E-02	5.28E-03
1.100E+10	253.8	253.9	+70.6	-55.8	255.2	+0.5%	+1.1%	1.32E-02	1.67E-02
1.150E+10	267.6	267.6	+83.4	-58.9	268.8	+0.5%	+1.0%	1.18E-02	1.66E-02
1.200E+10	281.7	281.7	+96.7	-67.6	282.6	+0.3%	+0.7%	1.06E-02	1.52E-02

See text for more information on the tabulated quantities. NC means "Not Converging."

### HMW-PE 3.25mm



## 6.4 Conclusions

Although soft boundaries form an electromagnetic superior solution for reducing the RCS resulting from edge diffracted waves, isotropic surface wave absorbers remain useful in many applications, even for RCS management of edge diffracted waves.

A new measuring apparatus based on a partially filled rectangular waveguide has been developed for determining the attenuation constant and phase constant of plane surface waves propagating along metal-backed surface wave absorbing materials. Measurements were performed which validate this new measuring method.

## 6.5 References

- [1] H. M. Barlow and A. L. Cullen, "Surface waves," *Proceedings of the Institution of Electrical Engineers*, Vol. 100, Part III, No. 68, Nov. 1953, pp. 329-347
- [2] W. M. G. Fernando, H. E. M. Barlow, "An investigation of the properties of radial cylindrical surface waves launched over flat reactive surfaces," *Proceedings of the Institution of Electrical Engineers*, Vol. 103, Part B, May 1956, pp. 307-318
- [3] F. C. Smith and S. Stroobandt, "The measurement of surface wave attenuation," *Progress Report*, The University of Hull (U.K.)
- [4] H. Jasik, *Antenna Engineering Handbook*, McGraw-Hill, 1<sup>st</sup> Ed., 1961, pp. 3.11-3.12
- [5] E. H. Scheibe, B. G. King and D. L. Van Zeeland, "Loss measurements of surface wave transmission lines," *Journal of Applied Physics*, Vol. 25, No. 6, June 1954, pp. 790-797
- [6] H. M. Barlow and A. E. Karbowski, "An investigation of the characteristics of cylindrical surface waves," *Proceedings of the Institution of Electrical Engineers*, Vol. 100, Part III, No. 68, Nov. 1953, pp. 321-328
- [7] K. Simonyi, *Theoretische Elektrotechnik*, Johann Ambrosius Barth, 10. Auflage, 1993, (in German), pp. 823-825
- [8] M. R. Spiegel, *Mathematical Handbook of Formulas and Tables*, Schaum's Outline Series, McGraw-Hill, 1968
- [9] HP 8510 Network Analyzer, *Operating and Service Manual*, Vol. 1, Operating and Programming, p. 166